Mon. Not. R. Astron. Soc. **000**, 1–26 (2004) Printed 5 September 2005 (MN LATEX style file v2.2)

Smoothed Particle Magnetohydrodynamics III. Multidimensional tests and the $\nabla \cdot \mathbf{B} = 0$ constraint

D.J. Price[1], J.J. Monaghan[2]
[1] *School of Physics, University of Exeter, Stocker Rd, Exeter EX4 4QL*
[2] *School of Mathematical Sciences, Monash University, Clayton 3800, Australia*

Submitted: 9th June 2005 Revised: 30th August 2005

ABSTRACT

In two previous papers (Price & Monaghan 2004a,b) (papers I,II) we have described an algorithm for solving the equations of Magnetohydrodynamics (MHD) using the Smoothed Particle Hydrodynamics (SPH) method. The algorithm uses dissipative terms in order to capture shocks and has been tested on a wide range of one dimensional problems in both adiabatic and isothermal MHD. In this paper we investigate multidimensional aspects of the algorithm, refining many of the aspects considered in papers I and II and paying particular attention to the code's ability to maintain the $\nabla \cdot \mathbf{B} = 0$ constraint associated with the magnetic field. In particular we implement a hyperbolic divergence cleaning method recently proposed by Dedner et al. (2002) in combination with the consistent formulation of the MHD equations in the presence of non-zero magnetic divergence derived in papers I and II. Various projection methods for maintaining the divergence-free condition are also examined. Finally the algorithm is tested against a wide range of multidimensional problems used to test recent grid-based MHD codes. A particular finding of these tests is that in SPMHD the magnitude of the divergence error is dependent on the number of neighbours used to calculate a particle's properties and only weakly dependent on the total number of particles. Whilst many improvements could still be made to the algorithm, our results suggest that the method is ripe for application to problems of current theoretical interest, such as that of star formation.

Key words: *(magnetohydrodynamics)* MHD – magnetic fields – methods: numerical – star formation

1 INTRODUCTION

Magnetic fields play an important, in some cases crucial, role in many areas of astrophysics. Despite the relative simplicity and well-studied nature of the equations which describe them, their effects are complicated and analytic studies are difficult and limited in scope. It is for this reason that a large theoretical effort over the past decade or so has been devoted to developing accurate numerical algorithms for Magnetohydrodynamics (MHD) in an astrophysical context. There are, however, severe technical challenges to be overcome in the numerical solution of the MHD equations.

Smoothed Particle Hydrodynamics (SPH, for a review see Monaghan 1992) is a fully Lagrangian particle method which solves the equations of fluid dynamics on a system of moving interpolation points which follow the fluid motion. SPH is an extremely versatile and robust numerical method and as a result has found widespread use in Astrophysics. There have, however, been difficulties with previous attempts to simulate magnetic fields within SPH, most prominently due to a numerical instability found to occur when an exactly momentum conserving form of the SPMHD equations was used.

In two previous papers (Price & Monaghan 2004a,b, hereafter papers I and II), we have described an algorithm for SPMHD in detail. The discrete equations are formulated from a variational principle (paper II) which ensures consistency with physical principles (such as conservation of momentum and energy) and a consistent treatment of magnetic divergence terms, the effects of which we will investigate in this paper. Artificial dissipation terms appropriate for shock-type problems were formulated in paper I. These terms are carefully formulated to give a positive definite contribution to the entropy. The algorithm has been tested on a wide range of standard one dimensional problems used to test recent grid-based MHD codes and also on the one dimensional 'Toy Stars' of Monaghan & Price (2004). The algorithm has been shown to give robust and accurate results on these problems.

In more than one spatial dimension errors associated with the non-zero divergence of the magnetic field need to be taken into account in any numerical MHD scheme. There are two distinct issues to be addressed. The first is the treatment of terms proportional to $\nabla \cdot \mathbf{B}$ in the MHD equations (in particular in the formulation of the induction equation and the magnetic force). The second is the maintenance of the $\nabla \cdot \mathbf{B} = 0$ constraint. It should be noted that a solution to the latter problem does not necessarily resolve the former, since maintaining $\nabla \cdot \mathbf{B} = 0$ in a particular numerical discretisation does not guarantee that it is zero in all discretisations.

With regards to the first issue, Brackbill & Barnes (1980) first noted that, when using a conservative formulation of the magnetic force, a supposed steady state could become polluted because of the small but non-zero component of magnetic force directed along the field lines due to a non-zero $\nabla \cdot \mathbf{B}$. This error can have serious consequences even though the proportional error in the magnetic field is small. In SPMHD the force parallel to the field in conservative formulations can have catastrophic consequences, leading to numerical instability under some circumstances (Phillips & Monaghan 1985). Brackbill & Barnes (1980) approached this problem by preferring a non-conservative formulation of the momentum equation which guarantees that the magnetic force is exactly perpendicular to the field. Such an approach has also been used successfully in an SPMHD context by several authors (e.g. Benz 1984; Meglicki et al. 1995; Byleveld & Pongracic 1996; Cerqueira & de Gouveia Dal Pino 2001), however numerical simulations of shocks seem to require the exact conservation of momentum in order to provide the correct jump conditions at shock fronts (which means, at the very least, the discrete formulation should be based on continuum equations which conserve momentum exactly even with a non-zero magnetic divergence).

This issue of neglect or inclusion of terms proportional to $\nabla \cdot \mathbf{B}$ was discussed at some length in paper I, where we followed both Janhunen (2000) and Dellar (2001) in formulating the MHD equations such that they form a consistent set in the presence of magnetic monopole terms, retaining both the conservation of momentum and energy necessary for shocks but using a 'non-conservative' formulation of the induction equation. The SPMHD equation set used in papers I was shown to form a consistent set with respect to the monopole terms in both discrete and continuum forms by deriving the SPMHD equations of motion and energy from a variational principle which uses the discrete formulations of the continuity and induction equations as constraints (see paper II). The implications of the formulation of the MHD equations in the propagation of divergence errors is discussed further in §6.1 and examined numerically in §7.2.

Many approaches to the second issue (namely the maintenance of the $\nabla \cdot \mathbf{B} = 0$ constraint) are possible. Perhaps the simplest in an MHD context is to explicitly evolve a vector potential $\mathbf{A}$, from which the magnetic field is derived by taking the curl, guaranteeing that the divergence is zero. The major disadvantage of this approach is that the computation of the force terms involves second derivatives of the evolved variable ($\mathbf{A}$), which in general can be significantly less accurate. Furthermore evaluation of dissipative terms proportional to $\nabla^2\mathbf{B}$ would require computation of the *third* derivatives. Whilst it may be possible to use the vector potential in an SPMHD context without degrading the accuracy substantially, we do not pursue such an investigation in this paper (although it is our intention to do so elsewhere).

Brackbill & Barnes (1980) proposed a simple projection scheme to 'clean up' the magnetic field at each timestep, an approach which is now commonly used in many grid-based MHD codes (e.g. Balsara 1998). Similar schemes have been implemented in an SPH context for the simulation of incompressible flows (Cummins & Rudman 1999). The disadvantage of this approach is that it involves the solution of a Poisson equation which is computationally expensive. In self-gravitating SPMHD this approach holds some promise as the cost may be mitigated by utilising the treecode used in the calculation of the gravitational force. In this paper we examine various projection methods based on this approach in §6.2.

Another approach used in grid-based MHD codes is the so-called 'constrained transport' method pioneered by Evans & Hawley (1988) in which differences of the magnetic field across the grid cell are constructed in such a way as to maintain the divergence free condition exactly. Such methods work very well, but is difficult to see how they can be made applicable to SPH because of the absence of a spatial grid (although perhaps some divergence-free interpolation could be devised). A comparison between several constrained-transport type schemes with the source term approach of Powell et al. (1999) and the projection method has been recently presented by Tóth (2000) for finite difference codes. Although not all of the schemes are applicable in an SPH context, many of the numerical tests presented in this chapter are taken from Tóth's paper.

More recently Dedner et al. (2002) have proposed a method for cleaning the magnetic field which is significantly faster than the projection method. This method involves explicitly adding a constraint propagation equation which is coupled to the evolution equation for the magnetic field. This equation propagates the divergence error in a hyperbolic (ie. wave-like) manner away from its source, allowing diffusion of the error to proceed rapidly within the timestep condition. This method is easily applied to the SPMHD algorithm and we provide details of the implementation in §6.3.

The paper is organised as follows: In §2 and §3 we summarise the formulation of the continuum MHD equations and the corresponding SPMHD form of these equations from papers I and II. In the course of the multidimensional testing, several aspects of the algorithm have been changed or refined from that presented in papers I and II. The first change is the method for removing the tensile instability, which is therefore discussed in §4. The implementation of the dissipative terms formulated in paper I in order to capture shocks (paper I) is reviewed and modified accordingly in §5. In §6 we investigate several of the approaches discussed above to the maintainance of the $\nabla \cdot \mathbf{B} = 0$ constraint which are applicable in an SPH context, namely the source term approach discussed in the previous chapter (§6.1), projection methods (§6.2) and the Dedner et al. approach (§6.3). The algorithm is then benchmarked, as in the one dimensional case, against a wide range of multidimensional test problems used to test recent grid-based MHD codes (§7).

The tests involve the propagation of an initially non-zero magnetic divergence (§7.2), nonlinear Alfvén waves (§7.3), two dimensional shock tubes (§7.5), an MHD rotor problem (§7.6) and the Orszag-Tang vortex (§7.7). The results are summarised in §8.

2 CONTINUUM EQUATIONS

Our SPMHD formalism is based on the equations of Magnetohydrodynamics in the form

$$\frac{d\rho}{dt} = -\rho\frac{\partial v^i}{\partial x^i}, \quad (1)$$

$$\frac{dv^i}{dt} = \frac{1}{\rho}\frac{\partial S^{ij}}{\partial x^j}, \quad (2)$$

$$\frac{de}{dt} = -\frac{1}{\rho}\frac{\partial (v_i S^{ij})}{\partial x^j}, \quad (3)$$

$$\frac{d}{dt}\left(\frac{B^i}{\rho}\right) = \frac{B^j}{\rho}\frac{\partial v^i}{\partial x^j}, \quad (4)$$

where

$$\frac{d}{dt} = \frac{\partial}{\partial t} + v^i\frac{\partial}{\partial x^i},$$

$$e = \frac{1}{2}v^2 + u + \frac{1}{2}\frac{B^2}{\mu_0\rho}, \quad (5)$$

$$S^{ij} = -P\delta^{ij} + \frac{1}{\mu_0}\left(B^iB^j - \frac{1}{2}\delta^{ij}B^2\right). \quad (6)$$

The formulation of these equations with respect to terms proportional to the divergence of the magnetic field was discussed in paper I and derived self-consistently from a variational principle in paper II. The implications of this particular formulation of the continuum equations in the propagation of divergence errors is discussed in §6.1 and confirmed in the numerical tests presented in §7.

Note that in place of the specific total energy e, the thermal energy can be evolved according to

$$\frac{du}{dt} = -\frac{P}{\rho}\frac{\partial v^i}{\partial x^i}. \quad (7)$$

Similarly, in place of (4) we could equivalently evolve the magnetic flux density B^i according to

$$\frac{dB^i}{dt} = -B^i\frac{\partial v^j}{\partial x^j} + B^j\frac{\partial v^i}{\partial x^j}, \quad (8)$$

The difference between evolving the total energy e in place of the thermal energy u is found to be very minor. One disadvantage of using the total energy is that it does not guarantee a positive thermal energy (although this can be a useful diagnostic of when a simulation is going wrong). We choose to evolve the magnetic flux per unit mass B^i/ρ since it is the natural variable to be carried by particles of fixed mass. Again, however, the difference between using (4) and (8) is found to be minor (although some difference might be expected for simulations involving large changes in the density). In general the differences between evolving different variables in SPH (and SPMHD) is dependent purely on the timestepping algorithm used and can be shown to decrease as smaller timesteps are used. It should be noted that these differences are much smaller than those found in grid-based codes due to the exact treatment of the advection terms in Lagrangian formulations.

The equation set is closed by an appropriate equation of state, which for an ideal gas is given by

$$P = (\gamma - 1)\rho u, \quad (9)$$

where P is the pressure, u represents the internal energy per unit mass and γ is the ratio of specific heats.

3 SPMHD EQUATIONS

The discrete formulation of the SPMHD equations was discussed in paper I and derived self-consistently from a variational principle in paper II. A self-consistent formulation of the SPMHD equations in the case of a variable smoothing length was also derived in paper II. We summarise the equations describing the method below.

The continuity equation is expressed by the density summation

$$\rho_a = \sum_b m_b W(|\mathbf{r}_a - \mathbf{r}_b|, h_a), \quad (10)$$

where $W(|\mathbf{r}_a - \mathbf{r}_b|, h)$ is the interpolation kernel with smoothing length h, for which we use the usual cubic spline (paper I, Monaghan 1992). The time derivative of (10) gives the SPH expression for the continuity equation (1), in the form

$$\frac{d\rho_a}{dt} = \frac{1}{\Omega_a}\sum_b m_b\mathbf{v}_{ab}\cdot\nabla_a W_{ab}(h_a), \quad (11)$$

where $\mathbf{v}_{ab} = \mathbf{v}_a - \mathbf{v}_b$ and Ω is a normalisation term which takes account of the variation of the smoothing length with density (paper II), given by[1]

$$\Omega_a = \left[1 - \frac{\partial h_a}{\partial \rho_a}\sum_c m_c\frac{\partial W_{ab}(h_a)}{\partial h_a}\right]. \quad (12)$$

The smoothing length is assumed to depend on the density via the relation

$$h_a = \eta\left(\frac{m_a}{\rho_a}\right)^{1/\nu}, \quad (13)$$

with derivative

$$\frac{\partial h_a}{\partial \rho_a} = -\frac{h_a}{\nu\rho_a}, \quad (14)$$

where ν is the number of spatial dimensions. We enforce this relation by calculating both h and ρ self-consistently by iteration of the density summation (10). The manner by which this is done is described in more detail in paper II and also in Price (2004). In brief, since the density of each particle is independent of neighbouring particle smoothing lengths we are able to iterate only those particles which have not converged. Furthermore we predict the new value of the smoothing length using the time derivative

$$\frac{dh_a}{dt} = -\frac{h_a}{\nu\rho_a}\frac{d\rho}{dt}. \quad (15)$$

As a result the additional cost involved is minimal.

[1] Beware that the expression given for Ω in paper II contains some typographical errors. The correct expression is given by (12).

The momentum equation (2) in SPH form is given by

$$\frac{dv_a^i}{dt} = \sum_b m_b \left[\left(\frac{S^{ij}}{\Omega\rho^2} \right)_a \frac{\partial W_{ab}(h_a)}{\partial x_a^j} + \left(\frac{S^{ij}}{\Omega\rho^2} \right)_b \frac{\partial W_{ab}(h_b)}{\partial x_a^j} \right], \quad (16)$$

whilst the energy equation (3) in discrete form is given by

$$\frac{de_a}{dt} = \sum_b m_b \left[\left(\frac{S^{ij}}{\Omega\rho^2} \right)_a v_b^i \nabla_a^j W_{ab}(h_a) + \left(\frac{S^{ij}}{\Omega\rho^2} \right)_b v_a^i \nabla_a^j W_{ab}(h_b) \right]. \quad (17)$$

The internal energy equation (7) in SPH form is given by

$$\frac{du_a}{dt} = \frac{P_a}{\Omega_a \rho_a^2} \sum_b m_b \mathbf{v}_{ab} \cdot \nabla_a W_{ab}(h_a). \quad (18)$$

Finally, the induction equation is given by

$$\frac{d}{dt}\left(\frac{B^i}{\rho} \right)_a = -\frac{B^j}{\Omega_a \rho_a^2} \sum_b m_b v_{ab}^i \frac{\partial W_{ab}(h_a)}{\partial x_a^j}, \quad (19)$$

or alternatively

$$\frac{dB_a^i}{dt} = -\frac{1}{\Omega_a \rho_a} \sum_b m_b \left[v_{ab}^i B_a^j - B_a^i v_{ab}^j \right] \frac{\partial W_{ab}(h_a)}{\partial x_a^j}. \quad (20)$$

4 INSTABILITY CORRECTION

In paper I an artificial stress or 'anticlumping' term described by Monaghan (1997) was used to eliminate the tensile instability associated with a conservative formulation of the momentum equation in SPMHD. The basis of this approach is that the instability manifests as particles clumping together in the presence of a negative stress and at short wavelengths (see below). The solution proposed by Monaghan (1997) and described in paper I was to introduce a repulsive term proportional to the anisotropic magnetic force which acts to remove the instability at short wavelengths by preventing particles from clumping together. This term has been used very effectively in elastic dynamics simulations (Gray et al. 2001) and was found to remove the instability very effectively in the one dimensional simulations considered in papers I and II. A more detailed investigation of the anticlumping term has been given recently in Price (2004), interpreting the anticlumping term as a modification of the kernel gradient used in the anisotropic force term. In this investigation several disadvantages to the anticlumping approach were highlighted. The first is that at large negative stresses (e.g. at low magnetic β) the anticlumping term can cause the numerical estimate of the sound speed to be significantly in error. The second, somewhat fatal disadvantage is that the anticlumping term does not appear to guarantee stability in the case of a variable smoothing length. For more details we refer the reader to Price (2004), however it suffices to say that the anticlumping approach does not appear to be uniformly satisfactory for dynamical MHD problems, particularly in more than one dimension. We therefore consider two alternative approaches in this paper, which are outlined below (§4.1,4.2).

It is worth recalling that the physical source of the instability is the additional small but non-zero force directed parallel to the magnetic field in the conservative formulation of the MHD equations (see introduction). For this reason it might be expected that enforcing the $\nabla \cdot \mathbf{B} = 0$ condition might also eliminate the tensile instability. In fact this is not the case, since the instability manifests even in one dimension (where the divergence is zero exactly). The reason for this is that although the divergence is zero by virtue of $B_x = \text{const}$, the gradient of this constant (as evaluated in the force term) is not necessarily zero numerically. In particular this is the case in the conservative formulation of the SPMHD equations, since the symmetric SPH gradient evaluation in the form

$$\nabla A_a = \sum_b m_b \left(\frac{A_a}{\rho_a^2} + \frac{A_b}{\rho_b^2} \right) \nabla W_{ab}, \quad (21)$$

is non-zero in the case of $A = \text{const}$. To counter this problem two approaches may be taken. The first is to add or subtract an arbitrary constant in order to keep the total stress positive and thus preventing negative stresses (and instability) from occurring. The second approach is to use an SPH gradient operator which vanishes for constant functions. These approaches are described below.

4.1 Removing the constant component of magnetic field

A simple method for removing the tensile instability is to subtract an arbitrary constant from the stress in order to make the total stress positive. For simulations where the magnetic field is strong due to an initial net flux through the system, a natural choice for this constant is to subtract the external (ie. produced by currents outside the simulation domain) component of the magnetic field. In this case the stress tensor (6) for particle a is modified according to

$$S_a^{ij} = -\left(P_a + \frac{1}{2\mu_0} B_a^2 \right) \delta^{ij} + \frac{1}{\mu_0} \left(B_a^i B_a^j - B_0^i B_0^j \right), \quad (22)$$

where $\mathbf{B}_0$ is the magnetic field component which does not change throughout the simulation (for example in one dimensional simulations we would use $\mathbf{B}_0 = [B_x, 0, 0]$). In general the constant field could also have a spatial profile (for example in a fixed dipole field from the central star in an accretion disc) in which case the analytic gradient could be used. In all of the cases we consider the external magnetic field is always the same independent of the particle position, such that calculating (22) involves storing only a single vector. It is worth noting that the formalism given above (where the constant field is subtracted from the total field) is more efficient than explicitly adding the contributions from separate constant and variable field components.

This simple solution completely cures the one dimensional instability because the B_x component of the field is explicitly removed from the anisotropic gradient term. Negative stresses can only arise in this formulation when the anisotropic terms in the fluctuating component dominate the isotropic pressure term (from which the constant field has *not* been subtracted).

A more general formulation which guarantees stability at all times must ensure that the total stress is positive. This can be achieved by using

$$S_a^{ij} = S_a^{ij} - S_{const}, \quad (23)$$

where

$$S_{const} = \max\left[\left(\frac{1}{2}\frac{B^2}{\mu_0} - P\right), 0\right]. \quad (24)$$

where the maximum is taken over all the particles. In many ways this is similar to the original proposal of Phillips & Monaghan (1985) in which the maximum value of the stress tensor over all the particles was determined and then subtracted from the stress for each particle. One disadvantage to this approach is that total energy is not conserved exactly since the contribution to the total energy evolution from the induction equation (which uses the total magnetic field) does not exactly balance the contribution from the momentum equation. An alternative is the approach of Morris (described below) in which the anisotropic term is modified slightly. In this paper we subtract the external field in simulations where a dominant external field is present, as in many of the two dimensional problems considered in this paper, reverting to the Morris approach otherwise. In practice we find little to differentiate the two approaches. The results in all cases are much better than those obtained using the anticlumping term.

4.2 Morris approach

An approach suggested by Morris (1996) is to retain the conservation of momentum on the isotropic terms in (16) but to treat the anisotropic terms using a differencing formalism which is exact in the case of a constant function (see above). The force term is then given by

$$- \sum_b m_b \left(\frac{P_a + \frac{1}{2}B_a^2/\mu_0}{\rho_a^2} + \frac{P_b + \frac{1}{2}B_b^2/\mu_0}{\rho_b^2}\right)\frac{\partial W_{ab}}{\partial x^i} \quad (25)$$

$$+ \frac{1}{\mu_0}\sum_b m_b \frac{(B_iB_j)_b - (B_iB_j)_a}{\rho_a\rho_b}\frac{\partial W_{ab}}{\partial x_j}. \quad (26)$$

This formalism does not therefore guarantee exact momentum conservation (since the anisotropic term does not give equal and opposite forces between particle pairs) but can be expected to give good results on shocks for which the anisotropic term is less important. It is also a better approach than using formalisms based on a pure $\mathbf{J}\times\mathbf{B}$ force since (26) is still a discretisation of a tensor force and therefore conserves momentum in the continuum limit for non-zero $\nabla\cdot\mathbf{B}$. This also means that (26) retains the consistent formulation of the MHD equations in the presence of monopoles, although the discrete equations are no longer self-consistent with each other (where self-consistent means that the equations can be derived from a variational principle and will thus conserve momentum, energy and entropy). Note that when using the variable smoothing length terms, we use the average of the normalised kernel gradient in (26), as in the dissipative terms. The small amount of non-conservation introduced by the Morris formulation is not found to significantly affect the shock capturing ability of the scheme.

5 DISSIPATIVE TERMS

Artificial dissipation terms which are required in order to simulate shocks were formulated in paper I. These terms are given by

$$\left(\frac{d\mathbf{v}}{dt}\right)_{diss} = -\sum_b m_b \frac{\alpha v_{sig}(\mathbf{v}_a - \mathbf{v}_b)\cdot\hat{\mathbf{r}}}{\bar{\rho}_{ab}}\nabla_a W_{ab}, \quad (27)$$

$$\left(\frac{d\mathbf{B}_a}{dt}\right)_{diss} = \rho_a\sum_b m_b \frac{\alpha_B v_{sig}}{\bar{\rho}_{ab}^2}(\hat{\mathbf{r}}\times(\mathbf{B}_{ab}\times\hat{\mathbf{r}}) r_{ab}F_{ab}, \quad (28)$$

$$\left(\frac{de_a}{dt}\right)_{diss} = -\sum_b m_b \frac{v_{sig}(e_a^* - e_b^*)}{\bar{\rho}_{ab}}\hat{\mathbf{r}}\cdot\nabla_a W_{ab}, \quad (29)$$

where

$$\hat{\mathbf{r}} = \frac{(\mathbf{r}_a - \mathbf{r}_b)}{|\mathbf{r}_a - \mathbf{r}_b|} \quad (30)$$

and

$$e_a^* = \begin{cases} \frac{1}{2}\alpha(\mathbf{v}_a\cdot\hat{\mathbf{r}})^2 + \alpha_u u_a \\ +\frac{1}{2}\alpha_B[B_a^2 - (\mathbf{B}_a\cdot\hat{\mathbf{r}})^2]/\mu_0\bar{\rho}_{ab}, & \mathbf{v}_{ab}\cdot\mathbf{r}_{ab} < 0; \\ \alpha_u u_a + \frac{1}{2}\alpha_B[B_a^2 - (\mathbf{B}_a\cdot\hat{\mathbf{r}})^2]/\mu_0\bar{\rho}_{ab}, & \mathbf{v}_{ab}\cdot\mathbf{r}_{ab} \geq 0; \end{cases} \quad (31)$$

with a similar expression for e_b^*. Note that the notation used in this paper differs slightly from that used in paper I. In particular we use separate parameters α, α_u and α_B to control the artificial viscosity, thermal conductivity and resistivity respectively rather than a single parameter K. Note also that these parameters are expected to be of order unity rather than $K\sim 0.5$ (such that α corresponds to the α used in the Monaghan (1992) artificial viscosity formulation used widely in SPH).

The signal velocity v_{sig} represents the fastest speed of signal propagation between the two particles. In MHD we use

$$v_{sig} = \frac{1}{2}\left[v_a + v_b - \beta\mathbf{v}_{ab}\cdot\hat{\mathbf{r}}\right], \quad (32)$$

where

$$v_a = \frac{1}{2}\left(\sqrt{c_a^2 + \frac{B_a^2}{\rho_a\mu_0} + \frac{2\mathbf{B}_a\cdot\hat{\mathbf{r}}c_a}{\sqrt{\rho_a\mu_0}}} + \sqrt{c_a^2 + \frac{B_a^2}{\rho_a\mu_0} - \frac{2\mathbf{B}_a\cdot\hat{\mathbf{r}}c_a}{\sqrt{\rho_a\mu_0}}}\right), \quad (33)$$

with a similar equation for v_b, where c is the sound speed. Again our notation differs slightly from that used in paper I as we use a dissipation parameter α of order unity and $v_{sig}\sim c_s$ (as opposed to $K\sim 0.5$ and $v_{sig}\sim 2c_s$ in paper I). The β term in the signal velocity in this formalism naturally provides the non-linear (Von Neumann-Richtmyer) component of the artificial viscosity.

The dissipative terms (27) and (28) provide an artificial viscosity and resistivity. The term involving $(u_a - u_b)$ in the energy equation provides an artificial thermal conductivity. These terms are derived so as to guarantee a positive definite contribution to the thermal energy and entropy (paper I). For reference the dissipative term added to the internal energy equation is given by

$$\left(\frac{du}{dt}\right)_{diss} = -\sum_b m_b \frac{v_{sig}}{\bar{\rho}_{ab}}\left\{\frac{1}{2}\alpha\left[(\mathbf{v}_a\cdot\hat{\mathbf{r}}) - (\mathbf{v}_b\cdot\hat{\mathbf{r}})\right]^2 + \alpha_u(u_a - u_b) + \frac{\alpha_B}{2\mu_0\bar{\rho}_{ab}}\left[B_{ab}^2 - (\mathbf{B}_{ab}\cdot\hat{\mathbf{r}})^2\right]\right\}\hat{\mathbf{r}}\cdot\nabla_a W_{ab} \quad (34)$$

In the one-dimensional tests described in paper I, it was found that the dissipative terms as described above were insufficient in shock problems involving jumps in the transverse velocity component, resulting in a modification of the viscosity term in order to apply the viscosity to all velocity components. This was attributed to the fact that the problems considered involved two and three dimensional velocity components whilst restricting the particles to move in only one spatial dimension. In the course of the multidimensional tests, it became apparent that this conclusion was incorrect. In paper I, following the usual procedure for hydrodynamical SPH, the dissipative terms were applied only for approaching particles ($\mathbf{v}_{ab}\cdot\hat{\mathbf{r}} < 0$). Whilst this is appropriate for the artificial viscosity term, discontinuities in the magnetic field (requiring artificial resistivity) can occur for particles in both compression and rarefaction. Applying the artificial resistivity (28) uniformly across the simulation was found to correct the oscillations observed in the magnetic field, and hence also in the transverse velocity components, removing the need for any modification of the viscosity term. In fact the results with the artificial resistivity term applied separately to the viscosity are an improvement on those given in paper I and are presented in Price (2004).

5.1 Dissipation terms using total energy

A further issue in a multidimensional context is that in the derivation of the above dissipative terms (paper I) it was assumed that only components of the magnetic field perpendicular to the line joining the particles would change at a shock front. However, in a multidimensional simulation the assumption of non-zero magnetic divergence may not hold exactly, as has already been discussed. In particular divergence errors are often created at flow discontinuities where fluid quantities are changing rapidly. It therefore makes good sense to drop the assumption of non-zero magnetic divergence in the derivation of the dissipative terms. The assumption that only the velocity components parallel to the line joining the particles will change is also not strictly true in MHD since velocity components transverse to this line will change with a jump in the transverse magnetic field. For this reason we re-derive the dissipative terms with an energy term of the form

$$e_a^* = \frac{1}{2}\alpha\mathbf{v}_a^2 + \alpha_u u_a + \alpha_B\frac{B_a^2}{2\mu_0\bar{\rho}_{ab}} \tag{35}$$

which involves both the total kinetic and magnetic energies. The implication is that smoothing is then also applied to jumps in $\mathbf{B}$ parallel to the shock (ie. $\nabla\cdot\mathbf{B}$ jumps) and via the kinetic term to transverse velocity jumps (ie. shear discontinuities). For the contribution to the entropy to be positive definite, the terms in the thermal energy equation must take the form

$$\left(\frac{du}{dt}\right)_{diss} = -\sum_b m_b\frac{v_{sig}}{\bar{\rho}_{ab}}\left\{\frac{1}{2}\alpha(\mathbf{v}_a-\mathbf{v}_b)^2 + \frac{\alpha_B}{2\mu_0\bar{\rho}_{ab}}(\mathbf{B}_a-\mathbf{B}_b)^2 + \alpha_u(u_a-u_b)\right\}\hat{\mathbf{r}}\cdot\nabla_a W_{ab}, \tag{36}$$

which correspondingly requires dissipation terms in the momentum and induction equations of the form

$$\left(\frac{d\mathbf{v}_a}{dt}\right)_{diss} = \sum_b m_b\frac{\alpha v_{sig}(\mathbf{v}_a-\mathbf{v}_b)}{\bar{\rho}_{ab}}\hat{\mathbf{r}}\cdot\nabla_a W_{ab}, \tag{37}$$

$$\left(\frac{d\mathbf{B}}{dt}\right)_{diss} = \rho_a\sum_b m_b\frac{\alpha_B v_{sig}}{\bar{\rho}_{ab}^2}(\mathbf{B}_a-\mathbf{B}_b)\,\hat{\mathbf{r}}\cdot\nabla_a W_{ab} \tag{38}$$

In the multidimensional case we find that use of (38) has distinct advantages over (28) since in more than one dimension divergence errors can cause the extra component of the magnetic field to jump slightly. Whether or not to use (37) in place of (27) is slightly less clear. The application of dissipative terms to specific discontinuities in a hydrodynamic context is discussed in Price (2004) with regards to artificial thermal conductivity, where it was found that smoothing of discontinuities in the thermal energy was necessary only where the discontinuity is not already smoothed by the application of artificial viscosity (which could occur, for example at a contact discontinuity). In the present case, since a jump in transverse velocity can *only* occur at a corresponding jump in the transverse magnetic field, these discontinuities will already be smoothed by the application of artificial resistivity there and so the use of (37) may simply result in excessive dissipation (since it must also be applied to particles in both compression and rarefaction, whereas the usual viscosity term is applied only to particles in compression). Furthermore (37) no longer conserves angular momentum (since the viscosity is not directed along the line joining the particles) and also no longer vanishes for rigid body rotation (since in effect rotational energy is converted into thermal energy). Thus for simulations involving significant amounts of shear (for example in accretion discs) the effects of using (37) would need to be studied quite carefully. It is worth noting that a similar term was used by Morris (1996) for SPMHD shocks in place of an artificial resistivity.

5.2 Dissipation switches

The artificial viscosity parameter α is controlled using the switch described in paper I (Morris & Monaghan 1997)

$$\frac{d\alpha}{dt} = -\frac{\alpha-\alpha_{min}}{\tau} + \mathcal{S} \tag{39}$$

In paper I we effectively used the source term

$$\mathcal{S} = \max(-2\nabla\cdot\mathbf{v}, 0.0) \tag{40}$$

which (as noted in paper I), is double the source term used by Morris & Monaghan (1997) (note that in paper I a dissipation parameter K is used which has a value of $\alpha/2$). In paper I it was found that the stronger source term was necessary in order to effectively damp post-shock oscillations. However for certain problems this source term could cause the artificial viscosity to become overly strong, resulting in excess smoothing of shock fronts. For this reason, in this paper we adopt a modification of the switch proposed by Rosswog et al. (2000), where the source term is given by

$$\mathcal{S} = \max(-\nabla\cdot\mathbf{v}, 0.0)(2.0-\alpha) \tag{41}$$

resulting in an initially stronger source term which tails off as α reaches its desired value of unity at the shock.

Since artificial resistivity is required at discontinuities in the magnetic field, which may occur where particles are not necessarily approaching each other, artificial viscosity and resistivity should not be controlled using the same switch, as was the case in paper I, leading to unnecessary modifications of the artificial viscosity term. A similar switch appropriate to the artificial resistivity term can be devised similar to that used in the viscosity. We evolve the resistive dissipation parameter α_B according to

$$\frac{d\alpha_B}{dt} = -\frac{\alpha_B}{\tau} + \mathcal{S} \tag{42}$$

where in this case the source term is given by

$$\mathcal{S} = \max\left(\frac{|\nabla \times \mathbf{B}|}{\sqrt{\mu_0 \rho}}, \frac{|\nabla \cdot \mathbf{B}|}{\sqrt{\mu_0 \rho}}\right), \tag{43}$$

which has dimensions of inverse time, as required by (42).

A similar switch may also be derived for the artificial thermal conductivity. A switch based on the first derivative of u was used in Price (2004). In this paper we use a switch based on the second derivative of u, where the source term is given by

$$\mathcal{S} = 0.1h|\nabla^2 u|, \tag{44}$$

where h is the smoothing length and we multiply the source term by a small number in order to apply only the very minimum amount of dissipation needed to eliminate the wall heating effect. The second derivative term is computed according to (e.g. Brookshaw 1985)

$$(\nabla^2 u)_a = 2\sum_b m_b \frac{(u_a - u_b)}{\rho_b} \frac{\mathbf{r}_{ab} \cdot \nabla_a W_{ab}}{\mathbf{r}_{ab}^2}, \tag{45}$$

The second derivative switch is preferable since it responds only to sharp discontinuities in u, ensuring that a minimal amount of artificial thermal conductivity is applied. Additionally it requires storage of fewer quantities than the switch involving the first derivative. We have not investigated the use of switches for artificial viscosity or resistivity based on second (or higher) derivatives in this paper although it deserves further study. In particular a switch based on $\nabla(\nabla \cdot \mathbf{v})$ would be very useful in self-gravitating simulations where $-\nabla \cdot \mathbf{v}$ can have large constant values in the absence of shocks due to the gravitational collapse.

6 DIVERGENCE CORRECTION TECHNIQUES

6.1 Source term approach

The induction equation can be written in the 'conservative' form

$$\frac{\partial \mathbf{B}}{\partial t} = -\nabla \times (\mathbf{v} \times \mathbf{B}), \tag{46}$$

$$= \nabla \cdot (\mathbf{v}\mathbf{B} - \mathbf{B}\mathbf{v}). \tag{47}$$

which explicitly conserves the volume integral of the flux

$$\int \mathbf{B} \mathrm{dV} \tag{48}$$

In Lagrangian form (46) can be written as

$$\frac{d\mathbf{B}}{dt} = -\mathbf{B}(\nabla \cdot \mathbf{v}) + (\mathbf{B} \cdot \nabla)\mathbf{v} + \mathbf{v}(\nabla \cdot \mathbf{B}). \tag{49}$$

Taking the divergence of this equation, we have

$$\frac{\partial}{\partial t}(\nabla \cdot \mathbf{B}) = 0, \tag{50}$$

showing that the constraint $\nabla \cdot \mathbf{B} = 0$ enters the MHD equations as an initial condition. However allowing magnetic monopoles resulting from $\nabla \cdot \mathbf{B} \neq 0$ to evolve appropriately within the flow can prevent the build up of unphysical numerical effects associated with their presence and can therefore reduce the need for computationally expensive divergence cleaning procedures. Thus Powell (1994) (see Powell et al. 1999) suggested that the conservative forms of the MHD equations should contain source terms to ensure that these errors are propagated out by the flow. With this in mind, Powell (1994) added source terms to the momentum, energy and induction equations, which take the (Lagrangian) form

$$\frac{dv^i}{dt} = \frac{1}{\rho}\frac{\partial S^{ij}}{\partial x^j} - \frac{B^i}{\rho}\frac{\partial B^j}{\partial x^j}, \tag{51}$$

$$\frac{de}{dt} = -\frac{1}{\rho}\frac{\partial (v_i S^{ij})}{\partial x^j} - \frac{v_i B^i}{\rho}\frac{\partial B^j}{\partial x^j}, \tag{52}$$

$$\frac{dB^i}{dt} = B^j \frac{\partial v^i}{\partial x^j} - B^i \frac{\partial v^j}{\partial x^j}. \tag{53}$$

Taking the divergence of (53) shows that the divergence errors in this formalism evolve according to

$$\frac{\partial}{\partial t}(\nabla \cdot \mathbf{B}) + \nabla \cdot (\mathbf{v} \nabla \cdot \mathbf{B}) = 0, \tag{54}$$

which has the same form as the continuity equation for the density (where in this case we have a density of magnetic monopoles, $\nabla \cdot \mathbf{B}$). This therefore implies that the total volume integral of $\nabla \cdot \mathbf{B}$ across the simulation is conserved and hence that the *surface* integral of the flux

$$\int \mathbf{B} \cdot \mathrm{dS} = \int (\nabla \cdot \mathbf{B}) \mathrm{dV}, \tag{55}$$

is conserved. The conservation of this quantity is far more important physically than the conservation of the volume integral (48).

The disadvantage of using (51)-(53) is that exact conservation of momentum and energy is sacrificed, which proves to be important for shock-type problems. Correspondingly it can lead to incorrect jump conditions at shock fronts (Tóth 2000). More recently it has been shown by Janhunen (2000) and Dellar (2001) that the correct formulation of the MHD equations in the presence of monopoles should *not* violate the conservation of momentum and energy.

The 'monopole formulation' of Janhunen (2000) and Dellar (2001) is identical to the self-consistent formulation of the SPMHD equations derived in paper II and given by (1)-(4). Note that the induction equation (8) (equivalently using (4)) is the same as in Powell's method and therefore the same conclusions can be drawn regarding the manner in which the divergence errors evolve (54). We investigate the implications of the 'source terms' in the induction equation in §7.2.

6.2 Projection methods

A common approach to the divergence problem is to clean up the magnetic field at regular intervals via the *projection method* (e.g. Brackbill & Barnes 1980). The basic idea

is to decompose the magnetic field into a curl and a gradient (which can be done unambiguously for any vector field) according to

$$\mathbf{B}^* = \nabla \times \mathbf{A} + \nabla\phi. \tag{56}$$

From this decomposition there are two ways of obtaining a divergence free field, both of which we discuss below.

6.2.1 Scalar projection

Taking the divergence of this expression results in the Poisson equation

$$\nabla^2\phi = \nabla \cdot \mathbf{B}^*, \tag{57}$$

which can then be solved for the scalar quantity ϕ. The magnetic field is then corrected according to

$$\mathbf{B} = \mathbf{B}^* - \nabla\phi. \tag{58}$$

The major disadvantage with this approach is that the solution of the Poisson equation (57) is computationally expensive, scaling as $\mathcal{O}(N^2)$. In an astrophysical SPH context this may be offset somewhat by the fact that the Poisson equation for the gravitational field is usually solved using a tree code (e.g. Hernquist & Katz 1989; Benz et al. 1990) which scales as $\mathcal{O}(N\log N)$. There are, however, some subtleties to this approach, which we outline below.

Projection schemes for incompressible flow in SPH have been implemented by Cummins & Rudman (1999), the results of which are applicable to the present case. The important point, also discussed by Tóth (2000) is that for the projection step to reduce the divergence to zero (ie. to provide an *exact* projection) requires that the discrete version of (57) is satisfied exactly. This means that the operator used to evaluate the divergence term on the right hand side of (57) should be the same as the divergence operator used in the evaluation of the ∇^2 on the left hand side and that the gradient operator used in the evaluation of ∇^2 should be the same as that used in (58). Cummins & Rudman (1999) approach this problem by calculating the ∇^2 using SPH operators, solving the Poisson equation by matrix inversion. Good results were also obtained using an approximate projection (ie. where the divergence operators on the left and right hand side differ). In this scheme Cummins & Rudman (1999) used the SPH evaluation of the Laplacian similar to that which is commonly used for thermal conduction in SPH (Brookshaw 1985; Cleary & Monaghan 1999) (and which is similar to the artificial thermal conductivity term used in this paper). The Poisson equation is then solved by inverting the resulting matrix equation.

The solution of (57) by direct summation (of which the tree code is an approximation), uses the exact solution to the Poisson equation (57) given by

$$\phi(\mathbf{r}) = \int G(|\mathbf{r}-\mathbf{r}'|)\nabla\cdot\mathbf{B}(\mathbf{r}')\mathrm{dV}(\mathbf{r}'), \tag{59}$$

where $G(|\mathbf{r}-\mathbf{r}'|)$ is the Green's function, given by

$$\begin{aligned} G(r) &= \frac{1}{2\pi}\ln r + \text{const}, \\ G(r) &= -\frac{1}{4\pi r}, \end{aligned} \tag{60}$$

in two and three dimensions respectively. The gradient needed in the correction step can be calculated directly, giving (in three dimensions)

$$\nabla\phi(\mathbf{r}) = -\frac{1}{4\pi}\int \frac{\nabla\cdot\mathbf{B}(\mathbf{r}')}{|\mathbf{r}-\mathbf{r}'|^3}(\mathbf{r}-\mathbf{r}')\mathrm{dV}(\mathbf{r}'). \tag{61}$$

In SPH we replace the volume element $\rho\mathrm{dV}$ with the mass per SPH particle and write the integral as a summation according to

$$\nabla\phi_a = -\sum_b m_b \frac{(\nabla\cdot\mathbf{B})_b}{4\pi\rho_b}\frac{(\mathbf{r}_a-\mathbf{r}_b)}{|\mathbf{r}_a-\mathbf{r}_b|^3}. \tag{62}$$

Since we still retain the freedom to choose the discrete operator used to evaluate $\nabla\cdot\mathbf{B}$ at each particle, it becomes clear that the solution by direct summation will only provide an *approximate* projection, since (57) is not discretely satisfied. This approximate solution will be degraded further when implemented using a tree code. A further disadvantage of the projection method for many of the problems considered in this paper is that it is somewhat complicated to implement in the case of periodic boundary conditions. The implication of these subtleties in the practical application of the projection method based on the Green's function solution (using a direct summation over the particles) are discussed in §7.2. Essentially we find that this projection method is reasonably effective at removing divergence errors at wavelengths larger than the smoothing length, but is less effective at removing short wavelength ($\sim h$) noise due to the smoothing of this noise inherent in the SPH operator used to calculate $\nabla\cdot\mathbf{B}$. Preliminary calculations using this projection method in conjunction with a tree code in three dimensions indicate similar results. In this paper we compute the divergence of the magnetic field using the SPH operator

$$(\nabla\cdot\mathbf{B})_a = -\frac{1}{\Omega_a\rho_a}\sum_b m_b(\mathbf{B}_a-\mathbf{B}_b)\cdot\nabla_a W_{ab}(h_a). \tag{63}$$

6.2.2 Vector projection

An alternative projection scheme can be implemented by solving for the vector potential $\mathbf{A}$. That is, we take the curl of (56) to obtain

$$\nabla\times\mathbf{B}^* = \nabla(\nabla\cdot\mathbf{A}) - \nabla^2\mathbf{A}. \tag{64}$$

Choosing the Gauge condition $\nabla\cdot\mathbf{A}=0$, we obtain a Poisson equation for the vector potential in terms of the current density $\mathbf{J} = \nabla\times\mathbf{B}^*/\mu_0$

$$\nabla^2\mathbf{A} = -\mu_0\mathbf{J} \tag{65}$$

with solution

$$\mathbf{A}(\mathbf{r}) = \int G(|\mathbf{r}-\mathbf{r}'|)\mathbf{J}(\mathbf{r}')\mathrm{dV}(\mathbf{r}'). \tag{66}$$

Taking the curl, we obtain an equation for the corrected magnetic field in terms of the current density, which in three dimensions is given by

$$\mathbf{B} = \nabla\times\mathbf{A} = -\frac{\mu_0}{4\pi}\int\frac{\mathbf{J}(\mathbf{r}')\times(\mathbf{r}-\mathbf{r}')}{|\mathbf{r}-\mathbf{r}'|^3}\mathrm{dV}(\mathbf{r}'). \tag{67}$$

which is simply Biot-Savart's Law. In SPH form this is given by

$$\mathbf{B}_a = -\sum_b m_b \frac{(\nabla \times \mathbf{B}^*)_b \times (\mathbf{r}_a - \mathbf{r}_b)}{4\pi\rho_b |\mathbf{r}_a - \mathbf{r}_b|^3}. \quad (68)$$

This method could also be useful in an SPH context in situations where several disconnected regions exist containing strong magnetic currents. By solving (67), the corrected magnetic field is determined from the current density, resulting in a knowledge of the magnetic field at any point in space. This approach was in fact used as the basis for the very first SPMHD algorithm implemented by Gingold & Monaghan (1977). In this paper we will only consider the use of 68 as a divergence cleaning method. In this respect solving (65) has a slightly higher computational expense than (62) since the Poisson equation is solved for a vector quantity rather than a scalar, giving (up to) three summations of $\mathcal{O}(N^2)$ as opposed to just one. Nevertheless, there is a significant difference between the two methods. The difference is that whereas the approximate nature of the projection in (62) means that the divergence is not guaranteed to be reduced to zero, in (68) the divergence of the expression for $\mathbf{B}$ *is* zero exactly by virtue of the curl in the summation.

The approximate nature of the projection in this case means that the current is not guaranteed to remain unchanged during the projection step. However (as noted by Monaghan 1992) the current is usually well estimated by the SPH particles since the current is in general where the matter is. In this paper we compute the current density using the SPH operator

$$(\nabla \times \mathbf{B})_a = -\frac{1}{\Omega_a \rho_a} \sum_b m_b (\mathbf{B}_a - \mathbf{B}_b) \times \nabla_a W_{ab}(h_a). \quad (69)$$

In practise we find that this projection method is far more effective than the scalar projection and this is demonstrated in §7.2 (see Figure 2). Again preliminary three dimensional calculations indicate similar results, although an implementation using the tree code is more difficult in this case since all three components of the vector potential must be stored and summed over the tree as opposed to just one in the scalar projection (in which case the standard gravity tree can simply be called with the source term replacing the particle mass). However the degree to which the physical current is affected by this projection in three dimensions remains to be investigated.

6.3 Hyperbolic divergence cleaning

Dedner et al. (2002) examine alternative divergence cleaning procedures. In their paper (see also Munz et al. 2000), they derive a general constrained formulation of the MHD equations, from which formalisms can be derived to give divergence cleaning which is elliptic (involving the solution of a Poisson equation), parabolic (in which the divergence errors are diffused away) and hyperbolic (where the divergence errors are propagated away from their source at a characteristic speed). The projection method described above is an elliptic approach, the main disadvantage to which is the substantial computational cost involved in the solution of the Poisson equation. The parabolic approach was found to be severely limited in scope due to the timestep restrictions imposed by the Courant condition[2]. The hyperbolic approach was found to be particularly effective, especially when combined with a parabolic term such that divergence errors are both transported and diffused. It is this approach that we outline below in an SPH context.

The basic idea is to introduce an additional scalar field ψ, which is coupled to the magnetic field by a gradient term in the induction equation,

$$\frac{d\mathbf{B}}{dt} = -\mathbf{B}(\nabla \cdot \mathbf{v}) + (\mathbf{B} \cdot \nabla)\mathbf{v} - \nabla\psi. \quad (70)$$

Note that our induction equation maintains the consistent treatment of divergence terms discussed above. The variable ψ is then calculated by adding an additional constraint equation, which for the combined hyperbolic/parabolic approach is given by

$$\frac{d\psi}{dt} = -c_h^2(\nabla \cdot \mathbf{B}) - \frac{\psi}{\tau}. \quad (71)$$

Neglecting the second term on the right hand side of (71) gives an equation for ψ which is purely hyperbolic. This implies that divergence errors are propagated in a wave-like manner away from their source with characteristic speed c_h (for more details we refer the reader to the Dedner et al. paper). The second term on the right hand side is a parabolic term which causes ψ to decay exponentially to zero with e-folding time τ (this is easily seen by neglecting the hyperbolic term and solving the resulting ordinary differential equation for $\psi(t)$). Since it is desirable for the divergence errors to be propagated at the maximum possible rate (within the timestep constraint imposed by the Courant condition), c_h should be set equal to the maximum signal propagation speed. For simplicity we calculate this as

$$c_h = \sqrt{\frac{\gamma P}{\rho} + \frac{1}{2}\frac{B^2}{\mu_0 \rho}}, \quad (72)$$

where the maximum value over all of the particles is used. The gradient term in the induction equation is calculated using a simple SPH estimate

$$\nabla\psi_a = \frac{1}{\Omega_a \rho_a} \sum_b m_b (\psi_b - \psi_a) \nabla_a W_{ab}(h_a). \quad (73)$$

Similarly the divergence of the magnetic field is calculated using (63).

The choice of decay timescale τ is more complicated. In Dedner et al. (2002) the decay timescale used is given by

$$\frac{1}{\tau} = \frac{c_h}{c_r} \quad (74)$$

where they find that an optimal cleaning on their chosen test problem is given by $c_r = 0.1$. The problem with this is that c_r is *not* a dimensionless parameter, but rather has units of length. Thus the optimal choice for any given problem will depend on the length scales in that particular problem. We explicitly write the timescale as

$$\frac{1}{\tau_a} = \frac{\sigma c_h}{\lambda_a}, \quad (75)$$

[2] an equivalent approach in SPMHD is to use an artificial resistivity in order to diffuse away divergence errors. This has been used, for example, by Morris (1996) and Hosking (2002).

where λ is a length scale and σ is a dimensionless parameter which determines the decay timescale. Setting $\sigma = 0$ therefore gives a purely hyperbolic correction. The physical interpretation of the length scale in the problem can be determined by solving the following reduced system of equations (ie. neglecting the usual MHD evolution terms)

$$\frac{\partial \mathbf{B}}{\partial t} = -\nabla\psi \quad (76)$$

$$\frac{\partial \psi}{\partial t} = -c_h^2(\nabla \cdot \mathbf{B}) - \frac{\psi}{\tau}. \quad (77)$$

Taking the divergence of the (76) and substituting into (77) we obtain the following equation for ψ

$$\frac{1}{c_h^2}\frac{\partial^2\psi}{\partial t^2} - \nabla^2\psi + \frac{\sigma\lambda}{c_h}\frac{\partial\psi}{\partial t} = 0 \quad (78)$$

where an identical equation may be obtained for the evolution of $\nabla \cdot \mathbf{B}$. This equation is simply the wave equation with a damping term, the solution to which is easily obtained by a separation of variables and is given in many standard textbooks. The length scale enters the solution as the wavelength for critical damping, that is the wavelength at which solutions change from being wave-like to being damped.

In practical calculations we expect divergence errors to be generated at wavelengths close to the smoothing length. We therefore set $\lambda = h$ and determine the value of the dimensionless parameter σ by experiment. A value of $\sigma = 0.2$ would imply that ψ (and thus $\nabla \cdot \mathbf{B}$) will have decayed significantly after the divergence errors have propagated approximately 5 smoothing lengths. In §7.2 we examine in detail the effects the hyperbolic cleaning on a problem involving a fixed wavelength of error (ie. independent of h) which graphically illustrates the divergence cleaning method (see Figure 3). The effect of this type of cleaning on errors generated by the flow are examined in §7.7. We find that values of $\sigma \sim 0.4-0.8$ generally give the best results, giving a good balance between the hyperbolic (fast but non-diffusive) and parabolic (diffusive but slow-acting) effects. In practise some diffusion is also added by the artificial resistivity terms (§5). In general, however, the divergence correction provided by the hyperbolic/parabolic scheme is found to be quite small (around a factor of ~ 2 reduction). Thus, whilst this type of divergence cleaning essentially comes free-of-charge computationally, under some circumstances it may be necessary to supplement it with a stronger form of cleaning, such as use of a projection method or some other kind of elliptic or parabolic cleaning which is not limited to the explicit time step condition.

7 NUMERICAL TESTS

The main issue to be addressed in 2D and 3D problems is the non-zero divergence of the magnetic field. In the SPH context it also allows us to estimate the extent to which the artificial dissipation spuriously affects the numerical results. Again there is a substantial literature of multi-dimensional MHD problems which have been used to test grid-based MHD codes (e.g. Dai & Woodward 1994; Ryu et al. 1995; Balsara 1998; Dai & Woodward 1998; Tóth 2000) and we consider several of these problems here.

7.1 Implementation

The implementation of the SPMHD equations used for the multidimensional tests is almost identical to that used in the one dimensional case (paper I). The density is calculated by summation, the total energy equation is used (although results are indistinguishable using the thermal energy equation in nearly all cases) and the magnetic field is evolved using (19) (or using (70) when using the hyperbolic cleaning). In the shock tube tests we use unsmoothed initial conditions. The artificial dissipative terms, except where otherwise indicated are implemented using the jump in total magnetic energy (§5.1) but the viscosity term uses only the velocity component along the line joining the particles (27). Unless otherwise indicated, artificial viscosity and thermal conductivity are applied using the switches discussed in §5.2 whilst the artificial resistivity term is applied uniformly using $\alpha_B = 1$. A major difference between the simulations presented here and those in the paper I is that the anti-clumping approach was not found to be uniformly successful in eliminating the tensile instability for all of the problems considered (in particular for the Alfvén wave test only a narrow range of parameters would produce stable results). Furthermore this term was found to result in spurious extra numerical noise, particularly in the shock tube tests. For this reason we have eliminated the tensile instability by simply subtracting the constant component of the magnetic field from the gradient term (§4.1) in the shock tube problems and using the stable Morris formulation of the magnetic force (§4.2) elsewhere. Note that even on the shock problems the differences in results between these two methods is almost negligible.

7.1.1 Error estimates

Various estimates can be made of the error produced in the simulation by any non-zero magnetic divergence. Monitoring these quantities over the course of a simulation thereby gives some measure of the magnitude of the error produced by $\nabla \cdot \mathbf{B}$. The most common approach in SPH implementations to date has been to monitor the dimensionless quantity

$$\frac{h\nabla \cdot \mathbf{B}}{|\mathbf{B}|} \quad (79)$$

and ensure that it remains small (typically < 0.01) over most of the simulation, where h is the SPH smoothing length and the divergence is calculated using (63). This provides some measure of the relative error in the magnetic field but no indication of how much influence this error has in the dynamics. For this reason it is also useful to measure the relative error in the total force caused by a non-zero divergence,

$$E_{force} = \frac{\mathbf{f}_{mag} \cdot \mathbf{B}}{|\mathbf{f}||\mathbf{B}|} \quad (80)$$

where $\mathbf{f}_{mag}$ is the magnetic component of the SPH force (16), whilst $\mathbf{f}$ is the total force on the particle. It is also useful to simply monitor the evolution in the maximum, minimum and average of $|\nabla \cdot \mathbf{B}|$ with time as well as various conserved quantities.

7.1.2 Conserved quantities

Aside from the usual conserved quantities of mass, momentum, angular momentum, energy and centre of mass, several additional quantities can be measured in MHD which can be useful diagnostics in a numerical simulation. A list of such quantities can be derived using Hamiltonian techniques and is given by (e.g.) Morrison & Hazeltine (1984). The helicity,

$$\int (\mathbf{A} \cdot \mathbf{B}) \mathrm{dV}, \tag{81}$$

where $\mathbf{B} = \nabla \times \mathbf{A}$, is a measure of the linkage of magnetic field lines (expressing the fact that magnetic field lines which are initially linked cannot become unlinked in the absence of dissipative terms). This quantity can only be usefully measured in simulations which explicitly use the vector potential $\mathbf{A}$. A similar invariant is the cross helicity

$$\int (\mathbf{B} \cdot \mathbf{v}) \mathrm{dV} \approx \sum_b m_b \frac{\mathbf{B}_b}{\rho_b} \cdot \mathbf{v}_b, \tag{82}$$

which measures the mutual linkage of magnetic field and vortex lines. The conservation of the cross helicity is a result of the magnetic field lines being frozen into the fluid. Measurement of the conservation of this quantity in a numerical simulation therefore provides an estimate of the degree of slippage of the magnetic field lines through the fluid. The volume integral of the magnetic flux (48) is also conserved across the simulation volume, provided that the flux is normal to (or zero at) the boundary of the integration volume. However the conservation of flux in a volume sense is not particularly important physically (Janhunen 2000). More important is that the surface integral of the flux (55) should be conserved. The conservation of these quantities with respect to formulations of the MHD equations in the presence of magnetic monopoles was discussed in §6.1.

There is also a conserved quantity which is the MHD analogue of the circulation (Bekenstein & Oron 2000; Kuznetsov & Ruban 2000), although the physical interpretation is somewhat obscure. It has been shown that SPH conserves an approximate version of the circulation in the hydrodynamic case (Monaghan & Price 2001), related to the invariance of the equations to the relabelling of particles around a closed loop due to the frozen-in vorticity field. A similar, though more restricted relabelling symmetry holds in the MHD case (in that the particles around the loop must also be on the same field line) and it may therefore be expected that SPMHD also maintains this invariance.

7.1.3 Visualisation

In order to make a direct comparison of our results with those of grid-based MHD codes, we interpolate the results from the particles to an array of pixels using the SPH kernel. That is, for a contour or rendered plot of a scalar quantity ϕ we interpolate to the pixels using

$$\phi(x, y) = \sum_b m_b \frac{\phi_b}{\rho_b} W(x - x_b, y - y_b, h_b) \tag{83}$$

where W is the cubic spline kernel used in the calculations (paper I; Monaghan 1992) and the summation is over contributing particles. Note that in practise this is quite simple to implement, as it involves only one loop over the particles, during which the contributions from the current particle to all pixels within a smoothing radius ($2h$) are calculated. For a vector quantity a similar interpolation can be performed for each component. An interactive plotting program incorporating these interpolation schemes for visualisation of SPH (and SPMHD) data in 1, 2 and 3 dimensions has been written by the author and is available upon request.

7.2 $\nabla \cdot \mathbf{B}$ advection

The first problem we examine is a simple test similar to that used by Dedner et al. (2002) in which a non-zero magnetic divergence is introduced into the simulation as an initial condition. This is a particularly good test for comparing various divergence cleaning procedures. The initial conditions are a uniform density distribution ($\rho = 1$) in the domain $-0.5 < x < 1.5, -0.5 < y < 1.5$ with a constant initial velocity field $\mathbf{v} = [1, 1]$. The initial gas pressure is $P = 6$ with $\gamma = 5/3$ and the magnetic field has a constant component perpendicular to the plane $B_z = 1/\sqrt{4\pi}$. The divergence is introduced as a peak in the $x-$component of the field in the form

$$B_x = (r/r_0)^8 - 2(r/r_0)^4 + 1 \qquad\qquad r = \sqrt{x^2 + y^2} \tag{84}$$

where r_0 is the radius of the initial peak. The setup used here differs from that used by Dedner et al. (2002) in that r_0 is a changeable parameter (using $r_0 = 1/\sqrt{8}$ gives their setup). The reason for this is that we find that the effectiveness of the divergence cleaning strongly depends on the wavelength of the divergence errors. Testing divergence cleaning procedures based on a single wavelength of error (as in Dedner et al. 2002) can lead to misleading interpretations and an incorrect choice of parameters when applied to divergence errors which are generated in the course of real simulations.

The contours of the initial B_x field arrangement (84) in the Dedner et al. (2002) case of $r_0 = 1/\sqrt{8}$ are shown in the left hand side of Figure 1 (and similarly in Figure 3). The particles are arranged on a cubic lattice for simplicity and in the evolution calculations the periodic boundary conditions are enforced using ghost particles. Since the density is uniform throughout the simulation the results are insensitive to whether $\mathbf{B}$ or $\mathbf{B}/\rho$ is evolved and also to the instability correction method since the simulation is not unstable to negative stress. The artificial dissipation terms are turned off for this problem in order to isolate the effects of the divergence cleaning procedures.

7.2.1 Projection methods

We use this problem to test the projection methods by applying a single projection step to the divergence error introduced in the initial conditions. To illustrate the divergence-free configuration adopted by the field we plot in Figure 1 the contours of B_x before and after the projection step. The initial configuration (left panel) is set according to (84) with $r_0 = 1/\sqrt{8}$, corresponding to that used by Dedner et al. (2002). The right panel shows the resulting field configuration after the projection step. We have used 2,500 (50×50) particles in this case, setup on a cubic lattice with a smoothing length set using $\eta = 1.2$ in (13), giving $h = 0.048$. This

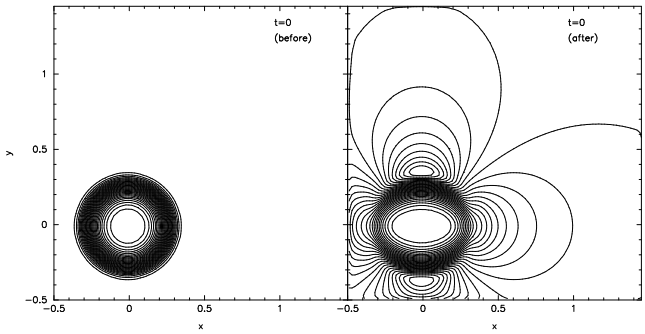

Figure 1. Divergence cleaning using the approximate (scalar) projection method described in §6.2. The plot shows 30 contours of B_x in the $\nabla\cdot\mathbf{B}$ advection problem before (left) and after (right) a single projection step at $t = 0$. The projected magnetic field adopts an essentially divergence-free configuration in a single step. Note that the wavelength of the initial divergence error in this case is substantially larger than the smoothing length.

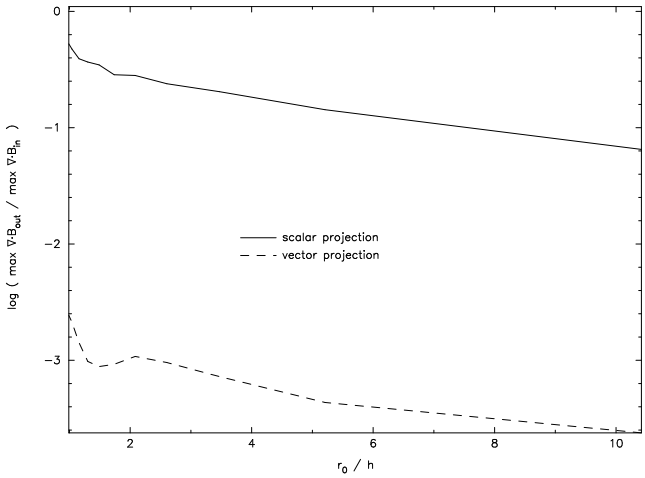

Figure 2. Wavelength dependence of the scalar and vector approximate projection methods described in §6.2. The $y-$axis shows the relative change in the maximum divergence error (ie. $\max(\nabla\cdot\mathbf{B}_{new}/\nabla\cdot\mathbf{B}_0)$ over a single projection step taken at $t = 0$. The $x-$axis gives the radius of the initial peak in the x component of the field r_0 in units of the smoothing length h. In both cases the projection step becomes less effective as the wavelength of the divergence error approaches the smoothing length (ie. $r_0/h \rightarrow 1$), however the vector projection outperforms the scalar projection by a factor of ~ 100 at all wavelengths.

means that the wavelength of the initial divergence error is substantially ($\sim 7\times$) larger than the smoothing length. However, we expect that divergence errors generated in the course of real simulations will tend to have wavelengths closer to $\sim h$. For this reason we have extended the test problem of Dedner et al. (2002) to a variety of wavelengths by varying the parameter r_0.

The relative divergence cleaning given from a single projection step using both the scalar (§6.2.1) and vector (§6.2.2) projection methods are plotted against r_0/h in Figure 2. The particles have been setup as previously, in this case varying r_0 whilst keeping h fixed. We have also performed simulations where r_0 is fixed and h is varied by changing the number of particles. The results in both cases are virtually identical. The results are also insensitive to the absolute size of the divergence error, since we plot only the relative change in $\nabla\cdot\mathbf{B}$.

For simplicity we have assumed that the boundaries are open when calculating the sum in the projection step, rather than explicitly treating the periodic boundaries. This is a reasonable assumption whilst the source terms for the Poisson equation (ie. $\nabla\cdot\mathbf{B}$ or $\nabla\times\mathbf{B}$) are non-zero in only a finite region of the simulation volume. However, to ensure that the maximum $\nabla\cdot\mathbf{B}$ value is not an artefact of our non-treatment of the periodic boundary conditions, the divergence near the boundaries of the domain (on particles within $2h$ of the boundary) has been set to zero when calculating the maximum used in Figure 2. These calculations shown in Figure 2 have also been performed with the B_x peak placed in the centre of the domain rather than at the origin in order to move the source further away from the boundaries.

It can be seen from Figure 2 that the effectiveness of the divergence cleaning given by the scalar projection is reduced as the wavelength of the divergence error approaches the smoothing length (for the scalar projection the reduction in error approaches a mere factor of ~ 2 as $r_0/h \rightarrow 1$). Whilst the vector projection (dashed line) shows a similar trend with wavelength, it is clear that this method is a vast improvement over the scalar projection, reducing the maximum divergence error by a factor of ~ 100 compared to the scalar case. This is due to the fact that the vector projection gives an expression for $\mathbf{B}$ which analytically has a zero divergence (refer to the discussion in §6.2.2). The only non-zero divergence resulting in this case is due to the SPH operator used to compute $\nabla\cdot\mathbf{B}$ after the projection step. This is therefore a substantial improvement over the scalar projection, in which $\nabla\cdot\mathbf{B}$ is not guaranteed to be exactly zero in *any* approximation. We have also experimented with the scalar projection using SPH operators for $\nabla\cdot\mathbf{B}$ other than (63), all of which we find show similar results.

7.2.2 Source terms and Hyperbolic/parabolic cleaning

The source term approach (§6.1) and the hyperbolic/parabolic cleaning (§6.3) are tested by evolving the initial field configuration given by (84) forward in time. The results of this test are shown in Figure 3. The plots show the divergence of the magnetic field as it evolves in each case. The results using the consistent formulation of $\nabla\cdot\mathbf{B}$ terms discussed in paper I and in §6.1 are shown in the top row. In this case the divergence error is passively advected by the flow and both the field and the divergence error remain unchanged (relative to the flow) at $t = 1$, demonstrating that the formalism is indeed consistent in the presence of magnetic monopoles and conserves the integral (55).

In order to compare these results with a conservative [in the sense of conserving (48)] formulation of the MHD equations, we have performed a simulation using an SPH induction equation of the form

$$\frac{d}{dt}\left(\frac{B_a^i}{\rho_a}\right) = \sum_b m_b\left[\frac{B_a^j}{\rho_a^2}(v_b^i - v_a^i) + \frac{v_a^i}{\rho_a^2}(B_b^j - B_a^j)\right]\frac{\partial W_{ab}}{\partial x_a^j} \quad (85)$$

which is an SPH form of the conservative (in a volume sense) induction equation

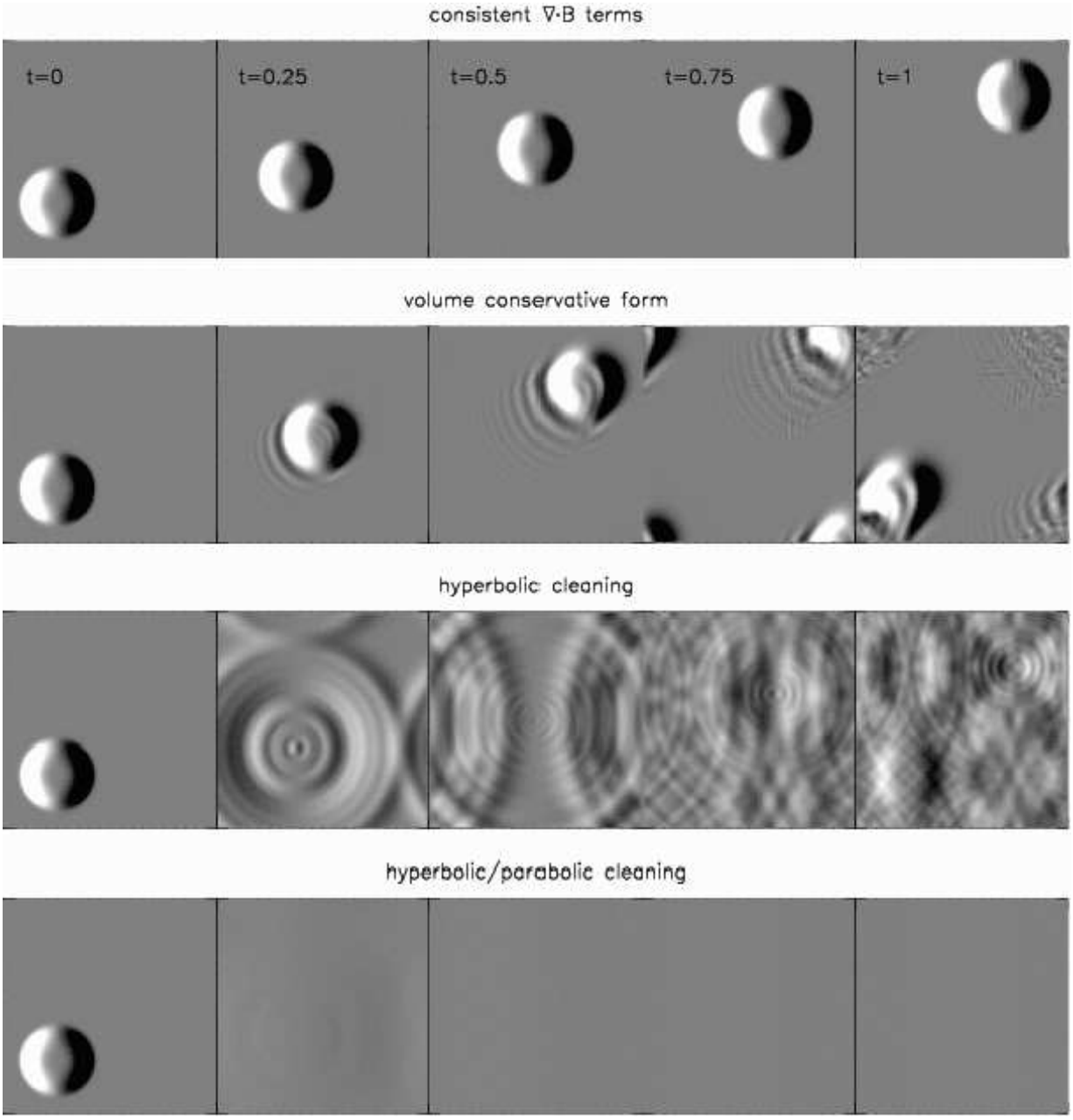

Figure 3. Results of the $\nabla \cdot \mathbf{B}$ advection problem. An initially non-zero divergence is setup as a peak in the $x-$component of the magnetic field (leftmost figures), with a velocity field $\mathbf{v}(x, y) = [1, 1]$ and periodic boundaries. The plots show renderings of $\nabla \cdot \mathbf{B}$ in the range $-1 < \nabla \cdot \mathbf{B} < 1$ (from black to white) at various times throughout the simulation for various divergence cleaning procedures. The consistent treatment of $\nabla \cdot \mathbf{B}$ terms (top row) is clearly seen to advect the divergence without change, which is an improvement over a "conservative" formulation of the MHD equations in which the divergence is smeared throughout the simulation volume (second row). With the use of hyperbolic cleaning in addition to the consistent $\nabla \cdot \mathbf{B}$ terms, the divergence error is spread rapidly in a wavelike manner (third row), whilst with a mixed hyperbolic/parabolic cleaning (fourth row) this error is also quickly diffused away.

$$\frac{d}{dt}\left(\frac{\mathbf{B}}{\rho}\right) = \left(\frac{\mathbf{B}}{\rho} \cdot \nabla\right)\mathbf{v} + \mathbf{v}\left(\frac{\nabla \cdot \mathbf{B}}{\rho}\right). \tag{86}$$

The results using this formalism are shown in the second row of Figure 3. The peak in B_x is distorted by the flow and the divergence error is smeared throughout the simulation.

The third row in Figure 3 shows the results using the divergence correction discussed in §6.3 using only the hyperbolic term in (71)(ie. with $\sigma = 0$) in conjunction with the usual monopole formulation of the induction equation (19). The divergence error is spread rapidly in a wavelike manner by the constraint equation. However, the magnitude does not decrease substantially in this case.

Using the mixed hyperbolic/parabolic cleaning with a small amount of diffusion (using the parabolic term in (71), in this case with $\sigma = 0.1$), this error is rapidly diffused away, resulting in a divergence-free field configuration (Figure 3, bottom row). For comparison, the results of a single pro-

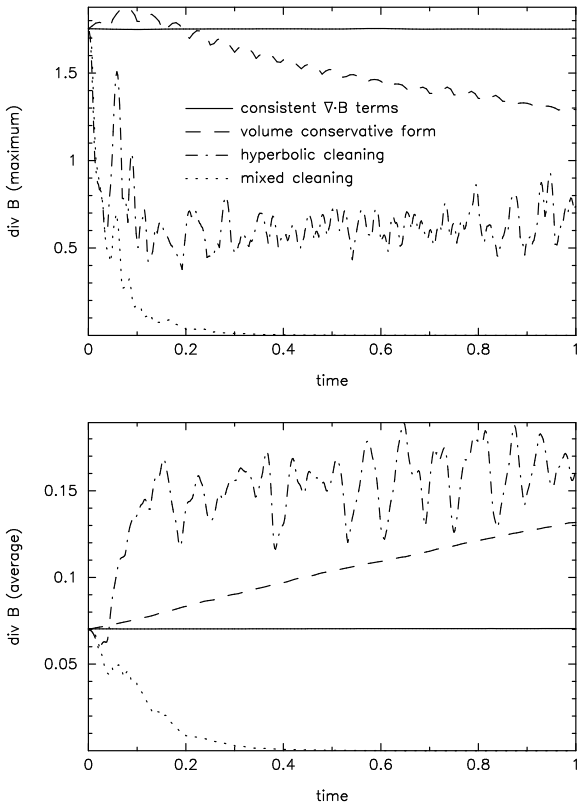

Figure 4. Time evolution of the maximum (left) and average (right) values of $|\nabla \cdot \mathbf{B}|$ over the particles. With a conservative formulation of the induction equation the divergence error increases with time (dashed line) whereas the errors are conserved using a formulation which is consistent in the presence of magnetic monopoles (solid line). With hyperbolic cleaning (dot-dashed) the maximum is quickly reduced although the average increases, however with the parabolic term included the average error is also rapidly diffused away (dotted line).

jection step at $t = 0$ are shown in Figure 1, showing the divergence-free configuration adopted by the field.

The time evolution of various quantities throughout these simulations are shown in Figure 4. The left panels show the evolution of the maximum (top) and average (bottom) of $|\nabla \cdot \mathbf{B}|$. In conservative form (solid line) the maximum divergence varies slightly and initially becomes larger than the initial value. The bottom panel shows that the average value in this case steadily increases over time, due to the smearing effect of the divergence propagation (50). The consistent formulation of $\nabla \cdot \mathbf{B}$ terms (dashed line) maintains a steady value of both the maximum and average, as observed in Figure 3. With hyperbolic cleaning (dot-dashed) the maximum divergence error is quickly reduced (although increases at later times as the divergence waves cross the periodic domain and interact) whilst the average climbs as the divergence error is spread throughout the domain. Using the mixed hyperbolic/parabolic cleaning as described above (dotted line), both the maximum and average divergence is swiftly reduced.

Finally it is important to examine the effect of varying the strength of the parabolic (diffusion) term in (71). The effects of varying the diffusion parameter σ for this particular

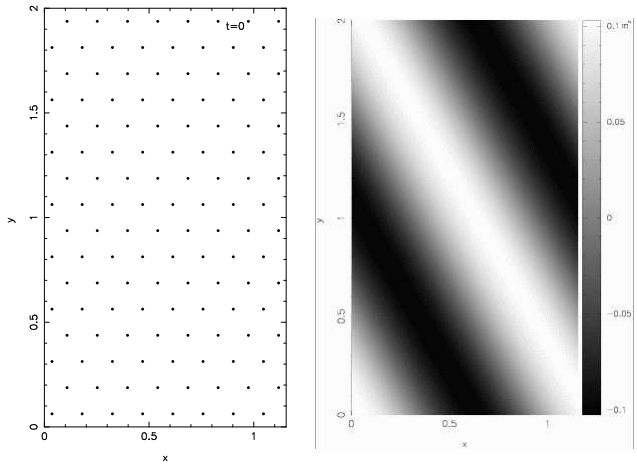

Figure 5. Circularly polarized Alfvén wave test. The left figure shows the particle setup in the lowest resolution simulation. On the right the vertical component of the magnetic field is plotted as a rendered image from the 32×64 particle run at $t = 5$, showing the propagation of the wave with respect to the domain and the particle setup.

problem were explored in Price (2004). It was later realised however that these results depended strongly on the value of the smoothing length (ie. the resolution of the calculations). Despite this the optimal parameter in other simulations was found to be independent of h. The reason for this is quite simple in hindsight and is due to our use of h as the length scale (wavelength of critical damping) in (75). In this test problem the divergence error is setup in the initial conditions at a wavelength r_0 which is independent of the actual resolution used. Thus using a length scale h in (75), the optimal cleaning is strongly dependent on resolution, since the optimal wavelength in this case corresponds closely to the wavelength of the initial divergence error. This also explains why Dedner et al. (2002) found that their use of a fixed parameter c_r which has dimensions of length was found to give cleaning which is independent of resolution (but only for this specific problem!). Since in realistic calculations divergence errors are produced at wavelengths $\sim h$, in general the length scale used in (75) should reflect this. We therefore retain the length scale h but defer examination of the effect of varying the parameter σ to the Orszag-Tang vortex problem (§7.7) where divergence errors are generated in the course of the evolution.

7.3 Circularly polarized Alfvén wave

This test is described by Tóth (2000) where it is used to test a variety of multidimensional MHD schemes in grid based codes. The test involves a circularly polarized Alfvén wave propagating in a two dimensional domain. The advantage of using a circularly (as opposed to linearly) polarized wave is that it turns out to be an exact, non-linear solution to the MHD equations, which means that the solution after one period should exactly match the initial conditions, without the effects of nonlinear steepening (as observed, for example, in the magnetosonic wave tests described in paper II). This also means that the wave can be setup with a much larger amplitude than would be used for purely linear waves.

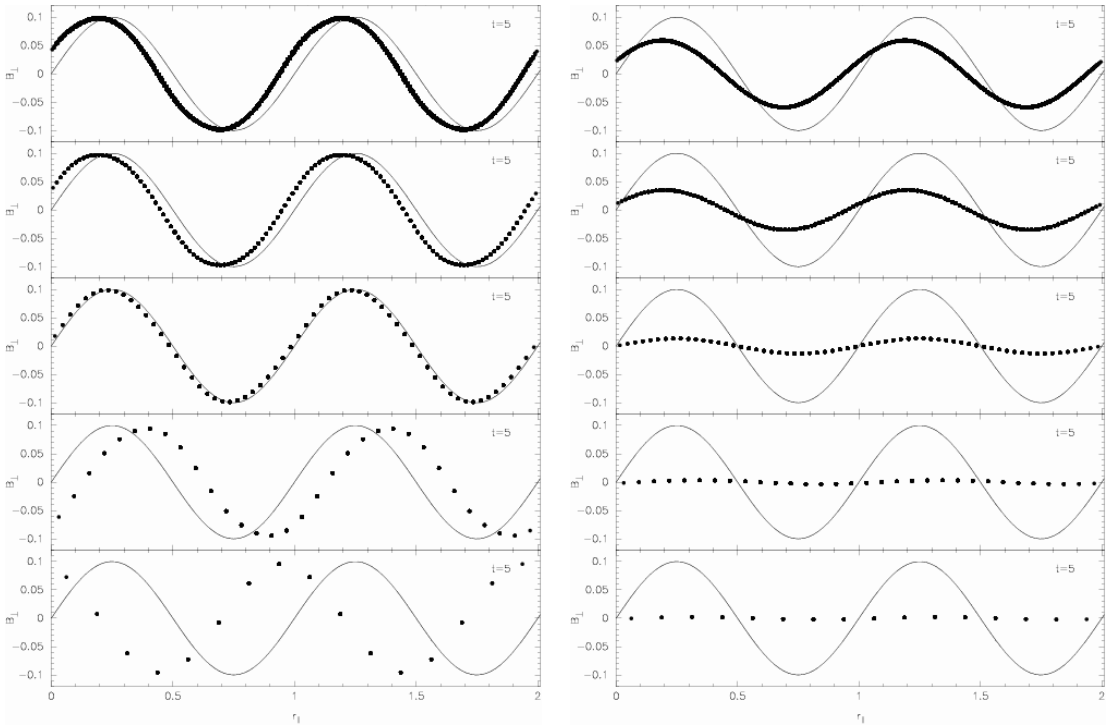

Figure 6. Results of the circularly polarized Alfvén wave test at $t = 5$ (corresponding to 5 wave periods). The plots show the perpendicular component of the magnetic field vector $B_\perp = B_y \cos\theta - B_x \sin\theta$ for all of the particles, projected against a vector parallel to the direction of wave propagation $r_\parallel = x\cos\theta + y\sin\theta$ (where $\theta = 30°$ in this case). The SPMHD results are shown at five different resolutions which are, from bottom to top, 8×16, 16×32, 32×64, 64×128 and 128×256. Initial conditions are indicated by the solid line. The numerical results should match these initial conditions at the time shown. The left panel shows the results in the absence of dissipative terms and demonstrates that the SPMHD algorithm contains very little intrinsic numerical dissipation even at low resolutions, although there is a small phase error present even in the converged higher resolution runs. The right hand panel shows the results applying the dissipative terms required in the shock tube problems uniformly (ie. in the absence of switches). In this case the wave amplitude is damped by the artificial resistivity term and exhibits somewhat slow convergence.

In Tóth (2000), the wave is setup to propagate at an angle $\theta = 30°$ with respect to the $x-$axis. In SPH the orientation of the wave vector with respect to the co-ordinates is not particularly important because there is no spatial grid. However, we have retained the rotated configuration as firstly it ensures that there are no spurious effects resulting from the initial arrangement of the particles and secondly enables a fair comparison with the results shown in Tóth (2000). The particles are setup on a hexagonal close packed lattice (ie. such that particles are equispaced) in a rectangular domain $0 < x < 1/\cos\theta; 0 < y < 1/\sin\theta$. This positioning of the boundaries means that periodic boundary conditions can be used, although some care is required to ensure the continuity of the lattice across the boundaries. This is achieved by stretching the lattice slightly in the $y-$direction to ensure that the boundaries lie at exactly half the spacing of the rows in the lattice. The particle setup at the lowest resolution is shown in the left hand side of Figure 5.

The wave is setup with a unit wavelength along the direction of propagation (ie. in this case along the line at an angle of 30° with respect to the x-axis). The initial conditions are $\rho = 1$, $P = 0.1$, $v_\parallel = 0$, $B_\parallel = 1$, $v_\perp = B_\perp = 0.1\sin(2\pi r_\parallel)$ and $v_z = B_z = 0.1\cos(2\pi r_\parallel)$ with $\gamma = 5/3$ (where $r_\parallel = x\cos\theta + y\sin\theta$). The $x-$ and $y-$ components of the magnetic field are therefore given by $B_x = B_\parallel \cos\theta - B_\perp \sin\theta$ and $B_y = B_\parallel \sin\theta + B_\perp \cos\theta$ (and similarly for the velocity). Conversely, $B_\parallel = B_y \sin\theta + B_x \cos\theta$ and $B_\perp = B_y \cos\theta - B_x \sin\theta$. Note that this setup means that $\nabla \cdot \mathbf{B} = 0$ holds as a combination of the $\partial B_x/\partial x$ and $\partial B_y/\partial y$ terms, rather than both components being zero individually. The vertical component of the magnetic field after 5 periods is plotted as a rendered image in the right hand side of Figure 5, showing the direction of wave propagation with respect to the domain and the particle setup.

We have peformed this test at five different resolutions: 8×16, 16×32, 32×64, 64×128 and 128×256 particles. In each case the number of particles in the y-direction is determined by the hexagonal lattice arrangement. The results are shown in Figure 6 after 5 wave periods (corresponding to $t = 5$). The plots show the perpendicular component of the magnetic field $B_\perp$ plotted against $r_\parallel$ for all of the particles in the simulation, with the results from the bottom to top panels shown in order of increasing resolution. In each case the initial conditions are indicated by the solid line which is identical to the exact solution at the time shown.

The left hand side of Figure 6 shows the results in the absence of dissipative terms (that is with the artificial viscosity, resistivity and thermal conductivity turned off). In this case the amplitude agrees very well with the exact solution even at the lowest resolutions. This demonstrates that SPH has a very low intrinsic numerical dissipation (compare for example with the damping of the wave at lower resolutions

in the plots shown in Tóth 2000). However there is a small phase error which remains even in the highest resolution run. This is similar to the phase error observed in the one dimensional sound wave tests presented in Price (2004) and in the one dimensional magnetosonic waves tests in paper I. In these cases the phase error was found to be essentially removed by accounting for the variable smoothing length terms (paper II). The results shown in Figure 6 incorporate the variable smoothing length terms, however in this case the phase error is not completely removed (although is still an improvement over the results using simple averages of the smoothing lengths or kernel gradients) unless a number of neighbours used is also increased in addition to the total number of particles.

The right hand side of Figure 6 shows the results of this test using the dissipative terms as required in the shock tube problems. In this case the wave is severely damped and convergence of the amplitude towards the exact solution is quite slow. The damping is largely caused by the uniform application of artificial resistivity (ie. using $\alpha_B = 1$ everywhere) resulting in a somewhat large dissipation even in the absence of shocks. Substantially improved results could be obtained using the resistivity switch discussed in §5.2, however for the shock tube problems it was found that use of such a switch could result in too little dissipation at rotational discontinuities in the absence of a shear viscosity term. Nonetheless the results shown in Figure 6 suggest that some kind of resistivity switch would be very valuable in SPMHD calculations. Note that the divergence error remains very small $\left[(\nabla \cdot \mathbf{B})_{max} \sim 10^{-3}\right]$ in all of the simulations shown even in the absence of any kind of divergence cleaning.

7.4 2.5D shock tube

The next two tests are simply two dimensional versions of the one dimensional shock tube tests described in paper I (see also Price 2004) and demonstrate the effects of divergence errors in the shock capturing scheme. In two dimensions we setup the particles on a cubic lattice in the $x-$direction in the domain $x = [-0.5 - v_{x(L)}t_{max}, 0.5 - v_{x(R)}t_{max}]$, where $v_{x(L)}$ and $v_{x(R)}$ are the initial velocities assigned to the left and right states. This means that at the time t_{max} the particles are contained in the domain $x = [-0.5, 0.5]$. The domain has a width of 4 particle spacings in the $y-$direction for computational efficiency. Boundary conditions are implemented by fixing the particle properties in two buffer regions at the edges of the $x-$domain, in which particles are evolved with a fixed velocity but copy their properties $(\rho, P, \mathbf{B})$ from the nearest 'active' particle. Periodic boundary conditions are used in the $y-$direction, implemented using ghost particles. The exact position of the $y-$boundary is chosen to ensure periodicity of the lattice arrangement, ie. at half the spacing of the initial rows of particles in the y-direction. The initial shock is setup as a discontinuity in the fluid quantities at $x = 0$ to which no smoothing is applied.

The first shock test is the adiabatic shock tube problem involving seven different discontinuities given in paper I. Strictly this is a '$2\frac{1}{2}$' dimensional problem since the transverse velocity and magnetic field also have components in the $z-$direction. Conditions to the left of the discontinuity (the left state) are given by $(\rho, P, v_x, v_y, v_z, B_y, B_z) = [1.08, 0.95, 1.2, 0.01, 0.5, 3.6/(4\pi)^{1/2}, 2/(4\pi)^{1/2}]$ whilst to the right (the right state) the conditions are $(\rho, P, v_x, v_y, v_z, B_y, B_z) = [1, 1, 0, 0, 0, 4/(4\pi)^{1/2}, 2/(4\pi)^{1/2}]$ with $B_x = 2/(4\pi)^{1/2}$ everywhere and $\gamma = 5/3$. The problem has been studied by in one dimension by many authors (e.g. Ryu & Jones 1995; Balsara 1998) and in two dimensions by Tóth (2000) and Dedner et al. (2002).

The problem was computed using 310×4 particles which corresponds to particles being uniformly spaced on a cubic lattice with separation 0.004 (with a slightly larger spacing for $x > 0$ to give the density contrast), although results are similar using a hexagonal close packed lattice arrangement. Note that the above figure refers to the number of particles in the domain $-0.5 < x < 0.5$ at $t_{max} = 0.2$ and that the resolution in this domain is correspondingly lower at earlier times due to the inflow boundary condition. The resolution was chosen to be comparable to the resolutions used in Tóth (2000). The small density difference between the left and right states was setup by changing the lattice spacing slightly in the $x-$direction.

The solution using an initial smoothing length of $h = 1.2(m/\rho)^{1/2}$ is shown in Figure 7 at $t_{max} = 0.2$ and may be compared with the exact solution taken from Ryu & Jones (1995) (solid line) and with the one dimensional SPMHD results shown in Price (2004) and in paper I.

On the shock tests the most important physical aspects for a numerical algorithm are obtaining the correct physical states behind the shock fronts, since this represents the manner in which the gas is changed by the passage of the shock. Thus whilst the shock profiles shown in Figure 7 are not as sharp as those shown at comparable resolution in, for example Tóth (2000), the intermediate states are obtained correctly apart from some small oscillations observed in the transverse velocity components near the contact discontinuity and the very narrow spikes in the magnetic field and transverse velocities which are damped at this resolution by our use of artificial resistivity.

Whilst the damping due to artificial resistivity improves with resolution (and with the use of the resistivity switch – see Figure 9), the oscillations in transverse velocity are of more concern. It should be noted first of all that these oscillations are quite small and do not appear to affect the dynamics significantly (mainly because the jumps in the transverse velocity components are an order of magnitude less than the jump in v_x). However, the oscillations appear to result from a combination of three factors: the unsmoothed initial conditions, the fact that we do not explicitly apply any smoothing to the transverse velocity components and the effects of the small jumps in the $x-$component of the magnetic field.

To remove these oscillations two approaches can be taken: The first approach is to modify the artificial viscosity terms slightly in order to smooth the transverse velocity profiles. The dissipative terms used in order to capture shocks were discussed at length in paper I and in this paper in §5. In the one dimensional case the dissipation terms for MHD (comprising an artificial viscosity, artificial thermal conductivity and artificial resistivity) were derived assuming that jumps would only occur in components of the magnetic field transverse to the line joining the particles that jumps in velocity would only occur parallel to this line. Neither of these assumptions strictly hold in the shock tube problem shown

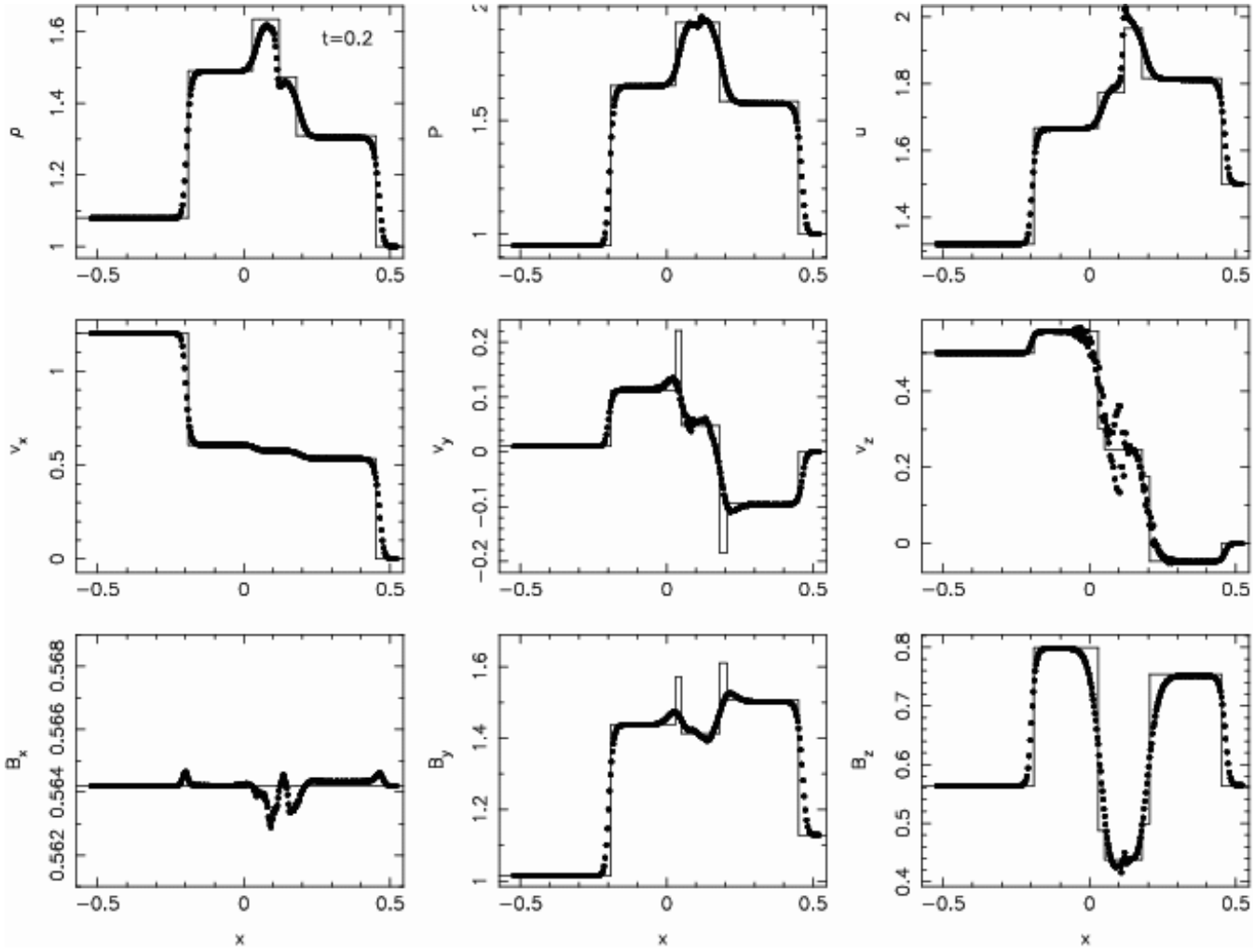

Figure 7. Results of the 2.5D shock tube test using 310×4 particles and an initial smoothing length of $h = 1.2(m/\rho)^{1/2}$. In two dimensions at this value of smoothing length small oscillations in the transverse velocity components appear primarily as a result of the non-zero magnetic divergence. In this plot the usual artificial viscosity and resistivity terms have been applied uniformly (ie. not using switches). A small amount of artificial thermal conductivity has been applied using the switch.

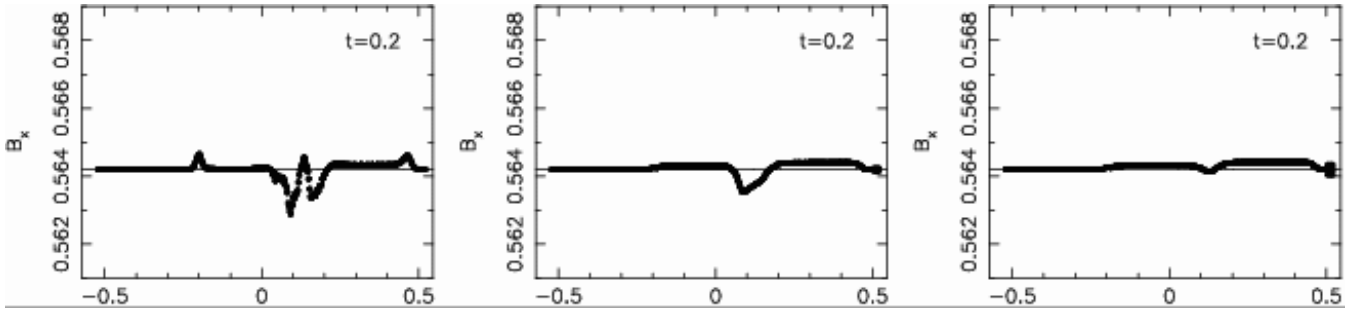

Figure 8. The parallel component of the magnetic field in the 2.5D shock tube problem using the usual dissipative terms (left), using the total magnetic energy (centre) and using the total magnetic and kinetic energies (right). Using the total magnetic energy in the dissipative terms means that jumps in the parallel field components are smoothed in addition to the jumps in transverse field. Using the total kinetic energy smooths jumps in the transverse (as well as parallel) velocity components, however this explicitly adds an undesirable shear component to the artificial viscosity term. Details of these formalisms are given in §5.

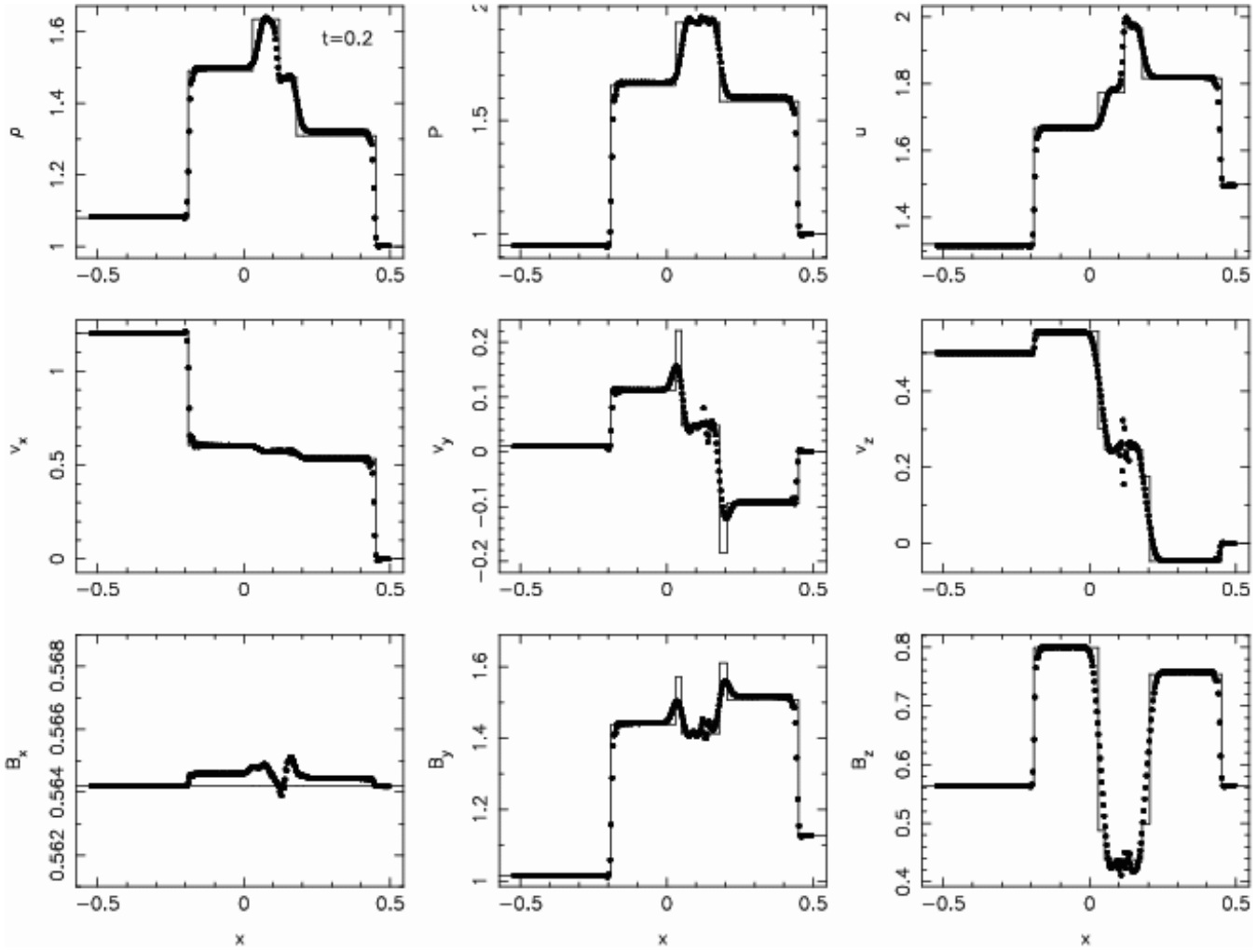

Figure 9. Results of the 2.5D shock tube test using 310×4 particles and an initial smoothing length of $h = 1.5(m/\rho)^{1/2}$ and the total magnetic energy in the artificial resistivity term but using the usual artificial viscosity term (where in this case both have been applied using the dissipation switches). The results are a substantial improvement on those presented in Figure 7 for a very modest increase in the number of neighbours.

in Figure 7 since the transverse velocity components clearly jump and there is also a small jump in the parallel field component due to the divergence errors.

A reformulation of the dissipative terms relaxing both of these assumptions was presented in §5.1, deriving the artificial viscosity and artificial resistivity terms from jumps in the total kinetic and magnetic energies respectively in the total energy equation. The effects of using these formulations on the profile of the parallel component of the magnetic field are shown in Figure 8. From the centre panel we see that using the total magnetic energy formulation for the artificial resistivity has clear advantages in preventing oscillations in the parallel component of the field at shock fronts. Using the total kinetic energy version of the artificial viscosity (in order to smooth out jumps in the transverse velocity) effectively adds an explicit shear component to the viscosity term.

In §5.1 it was noted that discontinuities in the transverse velocity components can only occur at corresponding jumps in the magnetic field and therefore that such discontinuities are already smoothed somewhat by the application of artificial resistivity there. For this reason the total kinetic energy formalism is not strictly necessary provided that there is sufficient artificial resistivity present to smooth both the transverse field jumps and the transverse velocity jumps. However, applying even a small amount of such a viscosity to the two dimensional problem is indeed found to remove the observed oscillations (Price 2004). It is clear though that the use of this term is highly undesirable since applying an explicit shear viscosity will substantially increase the spurious transport of angular momentum caused by the artificial viscosity term.

The second approach is to simply increase the number of neighbours slightly for each particle to give a more accurate interpolation. The results using an initial smoothing length of $h = 1.5(m/\rho)^{1/2}$ are shown in Figure 9 using the total magnetic energy formulation of the artificial resistivity but retaining the usual artificial viscosity formulation. In this case the jump in the parallel field component is much lower and the oscillations in the transverse velocity com-

ponents do not appear, although there is a small glitch at the contact discontinuity similar to that observed in the one dimensional case (Price 2004). The increase in smoothing length also means that the dissipative terms can be applied using the switches discussed in §5.2, resulting in a much lower dissipation rate away from the shocks than would be required for the $h = 1.2(m/\rho)^{1/2}$ case.

Increasing the smoothing length from $h = 1.2(m/\rho)^{1/2}$ to $h = 1.5(m/\rho)^{1/2}$ corresponds to an increase in the number of neighbours from ≈ 20 to ≈ 28 on a uniform cubic lattice in two dimensions. This quite a small increase in computational expense for a substantial gain in accuracy (and stability). It therefore seems much more desirable to increase the smoothing length slightly for multidimensional problems rather than to explicit add a shear viscosity term.

Finally, although this problem is not unstable to the clumping instability (and indeed no clumping is observed) we have also investigated the effects of various instability correction methods on the shock profile. In particular use of the anticlumping term (paper I) was found to produce additional noise in the shock profile. Using either the Morris formalism for the anisotropic force (§4.2) or subtracting the constant component of the magnetic field (§4.1) both give results very similar to those shown in Figures 7-9. Applying the hyperbolic/parabolic divergence cleaning to this problem gives a small reduction in the divergence error but otherwise has no significant effect on the shock profiles.

7.5 Two dimensional shock tube

The second shock tube test is used by both Tóth (2000) and Dedner et al. (2002) in two dimensions to compare the results of various divergence cleaning schemes, although the one dimensional version of this test has been used by many authors (e.g Dai & Woodward 1994; Ryu & Jones 1995). The results of the one dimensional test using the SPMHD algorithm are presented in Price (2004). Although this is a purely two dimensional test we present it after the 2.5D shock tube since it presents a much more challenging problem with regards to the non-zero divergence of the magnetic field due to the stronger shocks.

The particle setup is as described in the previous section, except that the initial left state is given by $(\rho, P, v_x, v_y, B_y) = [1, 20, 10, 0, 5/(4\pi)^{1/2}]$ and the right state is $(\rho, P, v_x, v_y, B_y) = [1, 1, -10, 0, 5/(4\pi)^{1/2}]$ with $B_x = 5.0/(4\pi)^{1/2}$ and $\gamma = 5/3$. The boundaries are correspondingly adjusted in the $x-$direction to allow the particles to fill the domain $-0.5 < x < 0.5$ at $t_{max} = 0.08$. Particles are arranged initially on a hexagonal lattice with particle spacing 0.004, giving 660 particles in the $x-$direction and a total particle number of $660 \times 4 = 2640$. As in the previous test, the results using an initial smoothing length of $h = 1.2(m/\rho)^{1/2}$ exhibit significant oscillations in the transverse velocity (v_y). In this case the oscillations are substantially worse because the jump in the parallel field component is much larger. Hence we have performed this test using $h = 1.5(m/\rho)^{1/2}$. However, even in this case the oscillations remain present and so we have also added the shear viscosity term, using (37) with $\alpha = 1$ everywhere (that is, not using the viscosity switch). The results using these settings are shown in Figure 10 and may be compared with the exact solution taken from Dai & Woodward (1994) (solid line) and with the one dimensional results given in Price (2004). All particles are shown projected along the $x-$direction. Even in this case some oscillations are visible in the v_y profile, corresponding exactly with a spike in $\nabla \cdot \mathbf{B}$. In the $h = 1.2(m/\rho)^{1/2}$ case this spike is much larger [$(\nabla \cdot \mathbf{B})_{max} \sim 40$], causing significantly more disruption to the velocity profile. Thus despite the various tweaks we have attempted for this test, the oscillations appear to be primarily caused by the divergence errors generated at the shocks. More importantly a slight offset in the intermediate states in the v_y, B_y, ρ and P profiles is present. Investigation of this effect suggests that this is caused by a combination of the divergence error and the shear viscosity term. Without the shear viscosity term the intermediate states *are* obtained correctly, although with substantially more oscillations in the v_y profile.

The effects of increasing the number of neighbours and changing the strength of the dissipation terms may be summarised as follows: Increasing the number of neigbours reduces the jumps in the parallel field component (for example with $h = 1.2(m/\rho)^{1/2}$ the jump is given by $\Delta B_x = [B_{x(max)} - B_{x(min)}]/B_{x0} \approx 18\%$ whilst for $h = 1.5(m/\rho)^{1/2}$ we have $\Delta B_x \approx 1\%$ and for $h = 2.4(m/\rho)^{1/2}$ this reduces further still to $\Delta B_x \approx 0.15\%$). On the other hand, adding dissipation at the jumps in parallel field means that although such jumps may be present, the discontinuities (causing strong divergence errors) are smoothed. The effect of adding the shear viscosity term is to increase the dissipation at these discontinuities, thus reducing to some extent the associated spike in the magnetic divergence.

In Tóth (2000) the results of this test were presented using the source term approach of Powell et al. (1999) (discussed in §6.1), showing similar jumps in the parallel magnetic field component which were unchanged even in the converged numerical results. The fact that the jumps in parallel field reduce with an increasing number of neighbours indicates that the SPMHD algorithm converges to the exact solution in the limit of $h \to \infty$ and $N \to \infty$ where N is the number of particles. Tóth (2000) attributes the errors in the parallel field components in the Powell method to the non-conservative source terms in the induction equation. We have also performed this simulation using the 'conservative' induction equation (85), however we find that the jumps in B_x are not changed significantly by including the $\mathbf{v}\nabla \cdot \mathbf{B}$ term (although contain substantially more numerical noise).

The shock tube tests presented above have been computed without using any form of divergence cleaning (other than the consistent formulation of the MHD equations in the presence of magnetic monopoles discussed in §6.1). Thus a way of eliminating both the jumps in parallel field and the resulting oscillations in the transverse velocity components is to clean up the divergence error. Using the hyperbolic/parabolic cleaning discussed in §6.3 is not particularly effective for this problem, since the divergence errors are propagated away from their source at the fastest wave speed which is similar to the rate at which they are created by the shocks. Thus the diffusion introduced by the parabolic term does not have time to eliminate the divergence error before oscillations in the velocity components are produced. This is illustrated in Figure 11 which shows the parallel field component and the divergence error after using this type of cleaning with $\sigma = 0.4$ in the parabolic term (c.f.

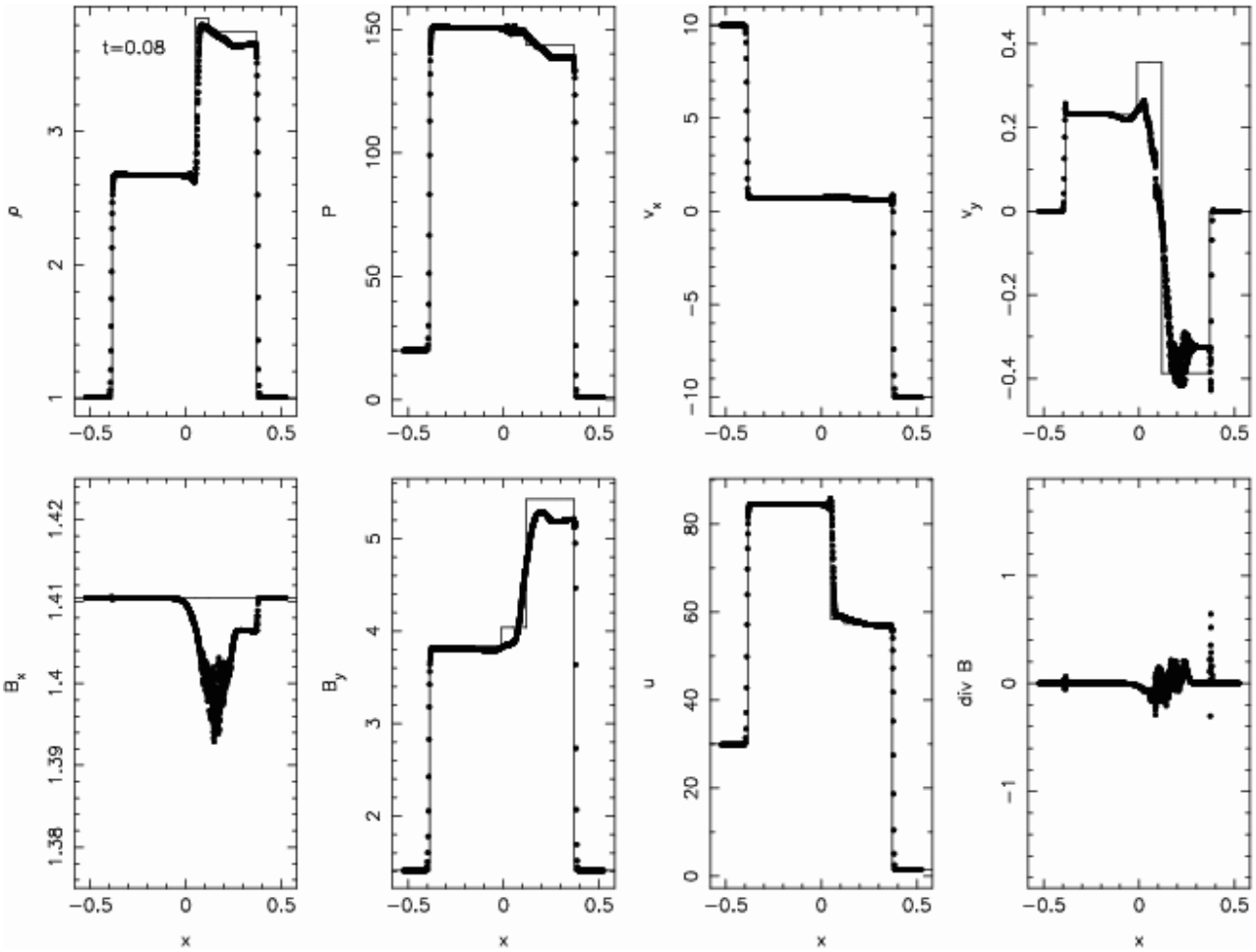

Figure 10. Results of the two dimensional shock tube test at $t = 0.08$ using $h = 1.5(m/\rho)^{1/2}$ and the shear viscosity term. The results may be compared with the exact solution given by the solid line. In this stronger shock tube problem the jumps in the parallel field can cause significant oscillations in the transverse velocity components due to the non-zero divergence terms.

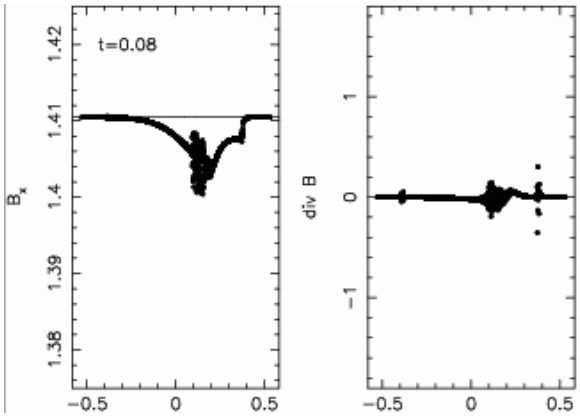

Figure 11. Parallel magnetic field (left) and the divergence error (right) in the two dimensional shock tube test at $t = 0.08$ computed as in Figure 10 but using the hyperbolic/parabolic divergence cleaning (§6.3). The exact solution is given by the solid line. The hyperbolic divergence cleaning does not have a large effect on this problem since the divergence errors are propagated at the fastest wave speed which is similar to the rate at which they are generated in the shocks.

§7.2). The divergence errors are reduced by a factor of ≈ 2 compared to the results shown in Figure 10. In order to eliminate the divergence errors from problems such as this one where divergence errors are created rapidly it seems necessary to invoke some kind of sub-timestep cleaning (such as a projection method). The implementation of such methods are complicated in this simple test problem by the use of periodic boundary conditions. Alternatively the number of neighbours can be increased further. To demonstrate this we present a simulation at double the usual neighbour number, that is using $h = 2.4(m/\rho)^{1/2}$. The results are shown at $t = 0.08$ in Figure 12 and show a reduction in the divergence error by a factor of ~ 10 compared to the results shown in Figure 10. This suggests that using a larger neighbour number may be crucial in three-dimensional SPMHD simulations.

7.6 Rotor

The next test is taken from Tóth (2000) and consists of a spinning, dense disc embedded in an ambient background medium containing a uniform magnetic field. The material initially contained within the disc is flung into the surround-

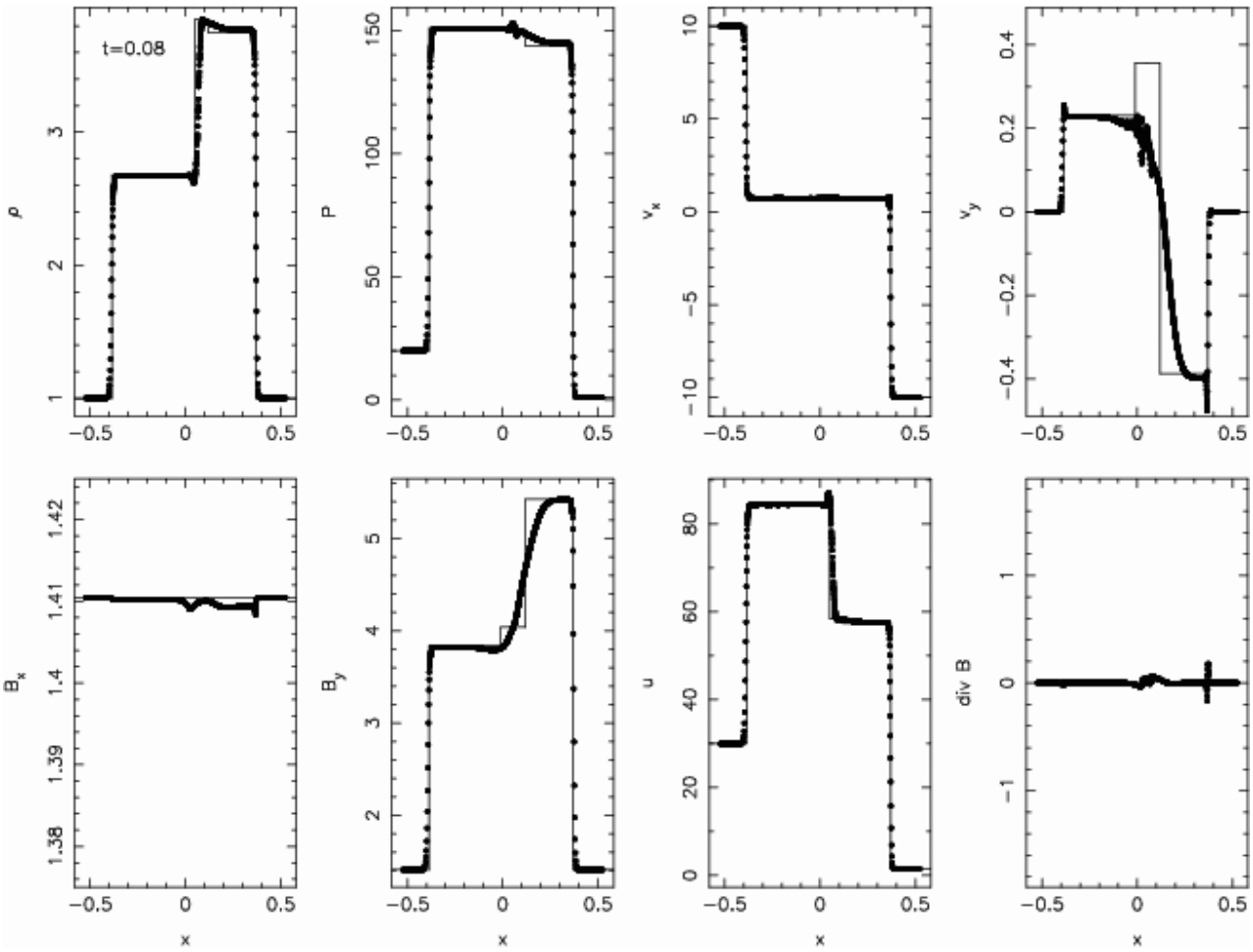

Figure 12. Results of the two dimensional shock tube test at $t = 0.08$ computed as in Figure 10 but using $h = 2.4(m/\rho)^{1/2}$. The exact solution is given by the solid line. Increasing the neighbour number significantly decreases the divergence error.

ing medium by the centrifugal forces, but is constrained into an oblate shape by the magnetic field. The computational domain is given by $-0.5 < x, y < 0.5$ with uniform thermal pressure $P = 1$ and an adiabatic index of $\gamma = 1.4$. A constant, uniform magnetic field is setup in the $x-$direction with strength $B_x = 5/\sqrt{4\pi}$. The dense disc is setup with $\rho = 10$ and a rotation velocity given by $v_x = 2(y - 0.5)/r_0$, $v_y = 2(x - 0.5)/r_0$ for $r < r_0$ where in this case $r_0 = 0.1$. The ambient medium is at rest with $\rho = 1.0$. Note that this choice of initial conditions corresponds to the 'first rotor problem' in Tóth (2000).

The density contrast between the disc and the background medium can be setup in SPH using either variable particle masses and therefore a fixed initial separation or equal mass particles and a variable particle distribution. We have experimented with both methods. In the variable particle mass case the large density contrast results in some spurious effects from the higher mass particles 'mixing' into the low particle mass medium and we therefore prefer the equal mass particle approach. We achieve this setup by setting up the initial disc with a dense concentration of particles setup on a regular, hexagonal close-packed lattice trimmed to $r < r_0$. The surrounding medium is then placed using a second close packed lattice with a correspondingly larger inter-particle separation with the region $r < r_0$ excluded. This setup means that we do not apply a taper function to the density, pressure or velocity profiles as in Tóth (2000). However the density profile is naturally tapered by the iterative calculation of the smoothing lengths and densities of the particles across the interface (§3). To ensure numerical pressure equilibrium we setup the thermal energy of the particles using $u_0 = P_0/[(\gamma - 1)\rho_0]$ after the initial density has been calculated by direct summation, rather than using the analytic density step. Despite this there are some initial transients but these do not appear to affect the subsequent evolution substantially.

The problem has been calculated using a background medium with 200 particles in the $x-$direction. The hexagonal lattice arrangement means that this corresponds to 200×230 particles in the surrounding medium, from which the central disc region is removed, leaving 44,332 particles in the background medium. The dense concentration of particles in the disc contains a further 14,454 particles, resulting in a total of 58,786 particles. Artificial viscosity and resistivity have been applied using the switches, with artificial thermal conductivity turned off. No divergence cleaning has been applied.

The results at this resolution using $h = 1.2(m/\rho)^{\frac{1}{2}}$

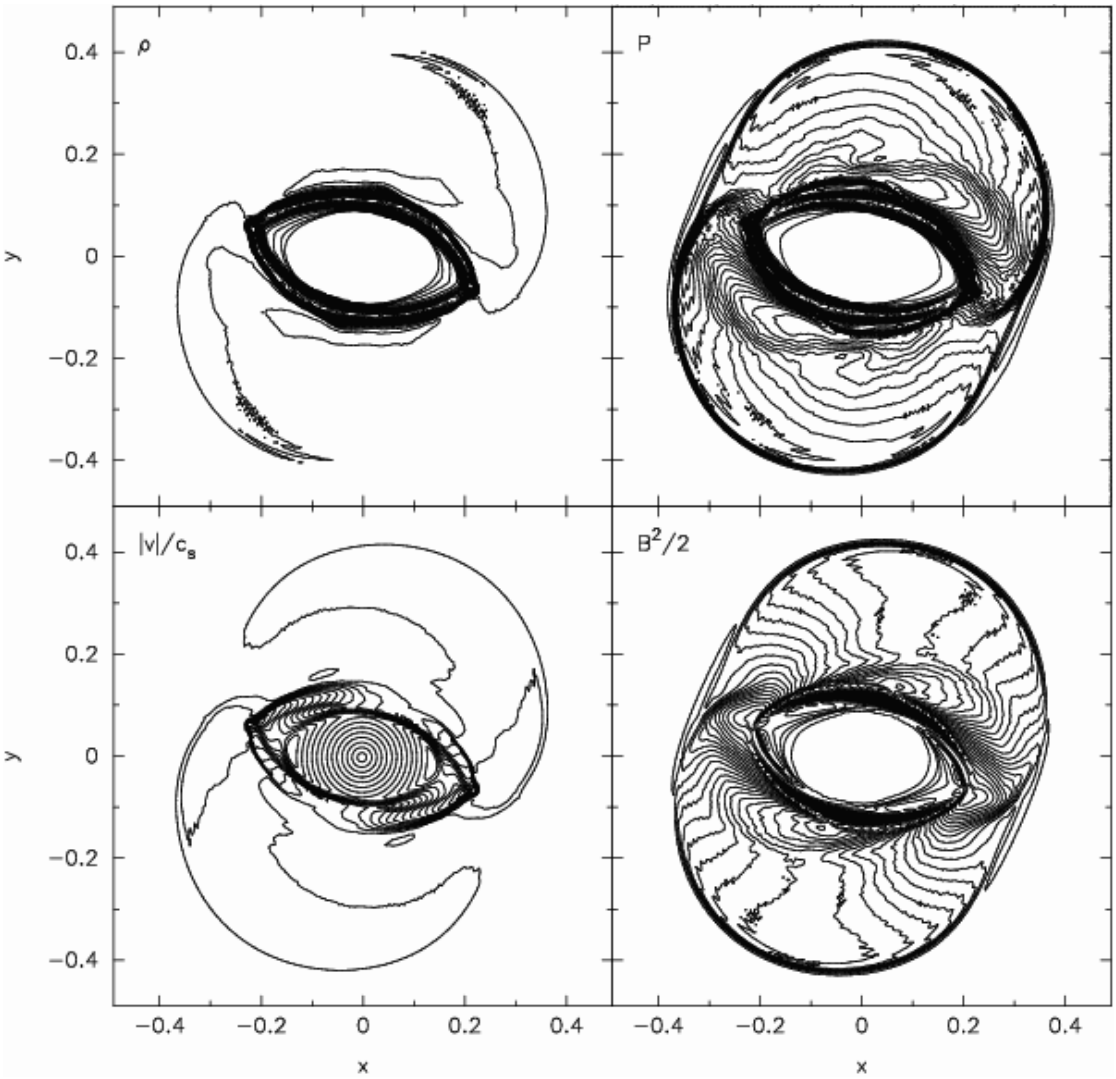

Figure 13. The density, pressure, mach number and magnetic pressure at $t = 0.15$ in the MHD rotor problem using 58,786 particles (roughly 200×200). All plots show 30 contours spaced between the limits given in Tóth (2000), that is $0.483 < \rho < 12.95$, $0.0202 < P < 2.008$, $0 < |v|/c_s < 1.09$, $0 < \frac{1}{2}B^2 < 2.642$ in order to make a direct comparison.

are plotted in Figure 13 and may be directly compared with the high resolution results shown in Tóth (2000). The density resolution in the SPMHD solution is slightly better than even the 400×400 grid based solution shown in Tóth (2000), giving a maximum density of $\rho_{max} = 15.54$ at $t = 0.15$ as opposed to $\rho_{max} = 12.95$ in the grid solution, although the minimum density at this time is $\rho_{min} = 0.74$ in the SPMHD solution as opposed to $\rho_{min} = 0.483$ in Tóth (2000). The SPMHD result using 400 particles in the $x-$direction (giving a total of 235,574 particles) resolves a density range of $\rho_{max} = 17.76$ and $\rho_{min} = 0.58$. The maximum field strength is a little lower in the SPMHD calculations, with $(\frac{1}{2}B^2)_{max} = 2.3$ (or 2.45 at the higher resolution), as opposed to $(\frac{1}{2}B^2)_{max} = 2.64$ in the 400×400 grid solution. This is due to our use of artificial resistivity for shock capturing. There are some small effects at low densities in the SPMHD solution due to the particle distribution. These effects decrease both with particle number and also as the number of neighbours is increased. The divergence constraint is maintained reasonably well in this problem – for example 95% of the particles have $h|\nabla \cdot \mathbf{B}|/|\mathbf{B}| < 0.01$ in the 200×200 particle simulation, which increases to 98% using 400×400 particles and decreases to 87% using 100×100 particles.

7.7 Orszag-Tang vortex

The final test is the compressible Orszag-Tang vortex problem which was first investigated by Orszag & Tang (1979) in order to study incompressible MHD turbulence. The problem was later extended to the compressible case by Dahlburg & Picone (1989) and Picone & Dahlburg (1991). More recently it has been widely used as a test problem for multidimensional MHD algorithms (e.g. Ryu et al. 1995; Balsara 1998; Dai & Woodward 1998; Londrillo & Del Zanna 2000; Tóth 2000).

The setup consists of an initially uniform density, periodic 1×1 box given an initial velocity perturbation

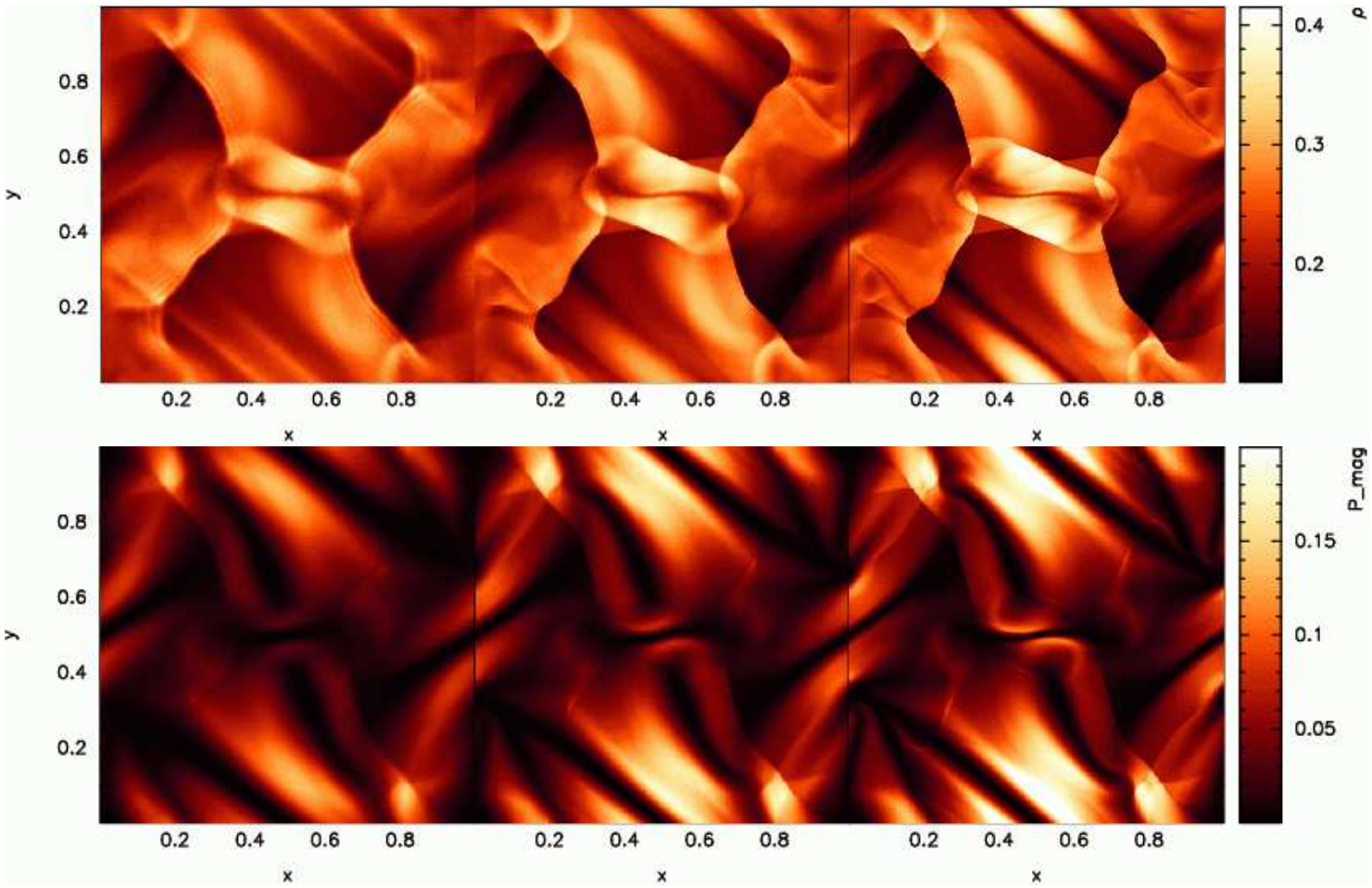

Figure 14. Results of the two dimensional Orszag-Tang vortex test, showing the density (top) and magnetic pressure (bottom) distributions at $t = 0.5$ for resolutions of 128×146 (left), 256×294(centre) and 512×590(right) particles. The particles are initially arranged on an isotropic hexagonal lattice with periodic boundary conditions. The initial velocity field is a large vortex $\mathbf{v} = [-\sin(2\pi y), \sin(2\pi x)]$ whilst the magnetic field has a doubly periodic geometry $\mathbf{B} = B_0[-\sin(2\pi y), \sin(4\pi x)]$. The SPMHD results at higher resolutions are in excellent agreement with those presented in (e.g.) Dai & Woodward (1998) and Tóth (2000).

$\mathbf{v} = v_0[-\sin(2\pi y), \sin(2\pi x)]$ where $v_0 = 1$. The magnetic field is given a doubly periodic geometry $\mathbf{B} = B_0[-\sin(2\pi y), \sin(4\pi x)]$ where $B_0 = 1/\sqrt{4\pi}$. The flow has an initial average Mach number of unity, a ratio of magnetic to thermal pressure of 10/3 and we use $\gamma = 5/3$. The initial gas state is therefore $P = 5/3B_0^2 = 5/(12\pi)$ and $\rho = \gamma P/v_0 = 25/(36\pi)$. Note that the choice of length and time scales differs slightly between various implementations in the literature. The setup used above follows that of Ryu et al. (1995) and Londrillo & Del Zanna (2000).

The particles are arranged initially on a uniform hexagonal close packed lattice. This distribution means that the particle are isotropically arranged and is the distribution towards which other arrangements naturally settle. However, results are similar using a cubic lattice arrangement. The simulation is performed at three different resolutions: 128×146, 256×294 and 512×590 particles (where the number of particles in the $y-$direction is determined by the isotropic lattice arrangement). The periodic boundary conditions are implemented using ghost particles. These resolutions are similar to the resolutions used in Dai & Woodward (1998) (although in SPH the resolution is concentrated preferentially towards regions of high density). The dissipation terms are applied using the artificial viscosity and resistivity switches but leaving the artificial thermal conductivity turned off in order to increase the density resolution. The wall heating effects which the artificial thermal conductivity prevents are discussed in Price (2004) and are in general quite minor. No shear viscosity term has been used. Simulations of this problem which have been run with or without the variable smoothing length terms, using the Morris formalism for the magnetic force (§4.2), evolving either $\mathbf{B}$ or $\mathbf{B}/\rho$ and either the thermal or total energy show essentially no difference in the numerical results.

The results of the density evolution are shown in Figure 14 at $t = 0.5$. At this time four main shock fronts are visible which have interacted in the central regions after having crossed the periodic domain. The SPMHD results, particularly are in good agreement with those presented in (e.g.) Dai & Woodward (1994, 1998) and Tóth (2000). In the lowest resolution run, the central regions appear to be slightly better resolved than in the 128×128 fixed-grid simulation of

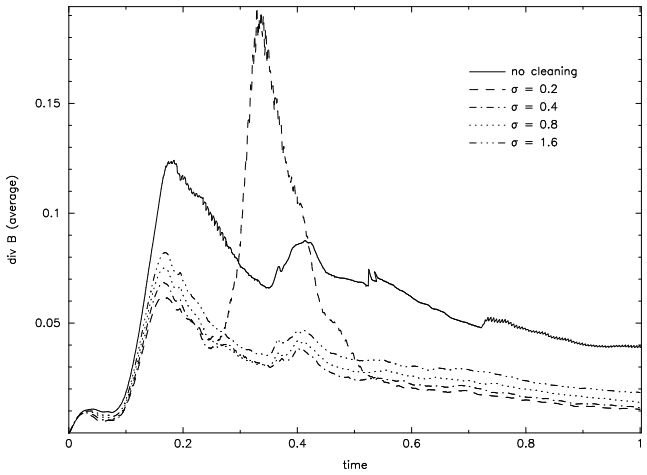

Figure 15. Effect of the hyperbolic/parabolic cleaning on the evolution of the average magnetic divergence in the two dimensional Orszag-Tang vortex problem, varying the parameter σ. With σ too low the cleaning can cause increases in $\nabla \cdot \mathbf{B}$ (dashed line) over simulations with no divergence cleaning (solid line). The optimal cleaning is obtained with $\sigma \sim 0.4 - 0.8$ (dot-dashed, dotted lines). However, the reduction in the divergence obtained using the hyperbolic cleaning is fairly small. The single biggest factor determining the magnitude of the divergence error is the number of neighbours. The results shown are for a smoothing length of $h = 1.2(m/\rho)^{1/2}$, although the errors decrease as the number of neighbours is increased.

Dai & Woodward (1998), although the lower density regions are correspondingly less well resolved. At this resolution the SPMHD solution shows some small residual effects due to the distortion of the initial regular particle arrangement, noticable as small ripples behind the shock fronts in Figure 14 and a slightly mottled appearance in the low density regions. This is particularly evident in Figure 14 since we have used a smoothing length of $h = 1.2(m/\rho)^{1/2}$. In the lowest resolution run the density maxima visible in the higher resolution runs at the top and bottom of the domain are largely washed out. This is a result of the artificial resisitivity term used for shock capturing which dissipates energy in these regions due to the strong current gradient.

The evolution of the average of the magnetic divergence is shown in Figure 15 for several runs using the hyperbolic divergence cleaning. The results using the hyperbolic/parabolic cleaning with $\sigma = 0.2$ (dashed line) can in fact increase the divergence error over the results with no divergence cleaning (solid line). This is because in the absence of sufficient diffusion the hyperbolic term can spread the divergence errors such that the resultant 'divergence waves' can constructively interfere with each other, leading to increased errors. The optimal cleaning is obtained with $\sigma \sim 0.4 - 0.8$ (dot-dashed, dotted lines), although the reduction in the divergence error given by the hyperbolic cleaning is comparatively small. In fact, as in the previous tests, the single biggest factor which determines the magnitude of the divergence error is the number of neighbouring particles. For example in a simulation using $h = 1.5(m/\rho)^{1/2}$ the divergence errors are approximately half those shown in Figure 15.

8 DISCUSSION

In this paper multidimensional aspects of the SPMHD algorithm have been discussed. In particular several methods for maintaining the divergence-free constraint in an SPH context have been presented. Firstly the source term approach of Powell et al. (1999) was outlined and contrasted with the consistent formulation of the MHD (and SPMHD) equations derived in paper II. The major difference between the two approaches is that our approach retains the conservation of momentum and energy whereas the Powell et al. approach does not. The conservation properties of the induction equation were also discussed, in which it was highlighted that using a 'non-conservative' induction equation means that the surface integral of the magnetic flux is conserved, rather than the volume integral. The effect of using the consistent formulation of the MHD equations in the presence of magnetic monopoles (which conserves the surface integral of the flux) is that divergence errors are advected without change by the flow (illustrated in Figure 3).

Projection methods for maintaining a divergence free field were discussed in an SPH context in §6.2. In particular it was noted that using the Green's function solution to the Poisson equation (as is often used for self-gravity in SPH) provides only an approximate projection. The results using this type of projection on a problem where an initial magnetic divergence was introduced into the simulation were very good (§7.2), but were found to degrade as the wavelength of the divergence error approached the resolution length. A projection method based on Biot-Savart's law was also discussed and found to give excellent results even for wavelengths approaching the smoothing length. The implementation of either of these projection schemes for the test problems considered in this paper was complicated by the periodic boundary conditions used, leaving a need for further testing of these methods on three dimensional problems. In particular the Biot-Savart projection method suggests a promising divergence cleaning method in three dimensions. This would however require implementation in a tree-code which is beyond the scope of this paper.

An alternative approach to divergence cleaning suggested recently by Dedner et al. (2002) was discussed in §6.3. The method involves adding an additional constraint equation which is coupled to the induction equation for the magnetic field. Chosen appropriately, the effect of this equation is to cause the divergence errors to be propagated in a wave-like manner away from their source (Figure 3). Adding a small diffusive term means that the divergence errors are also rapidly reduced to zero. This method is extremely simple to implement and is computationally very inexpensive. The disadvantage is that the error propagation is limited by the timestep condition and, although much faster than using diffusion alone to reduce the divergence, for some problems (for example the shock tube tests given in §7.4 and §7.5) the cleaning is still not fast enough. However, this method is some improvement over not using any form of divergence cleaning at a negligible additional computational cost.

The SPMHD algorithm was also tested against a variety of multidimensional test problems. A non-linear circularly polarized Alfvén wave was studied in §7.3. This test showed that SPMHD has a very low intrinsic numerical dissipation compared to grid based codes, although this property is de-

stroyed by the addition of explicitly dissipative terms for shock-capturing which can cause quite slow convergence on problems where the physical dissipation timescale is of critical importance.

Two of the shock tube problems examined previously in one dimensional simulations (paper I Price 2004) were examined in two dimensions in §7.4 and 7.5. For these problems jumps in the component of the magnetic field parallel to the shock front (causing divergence errors) were found to result in oscillations in the transverse velocity profiles. The jumps in the parallel field component were found to decrease as the number of neighbours for each particle was increased. The corresponding divergence errors produced by these jumps could be reduced by using a form of the dissipative terms derived in §5.1 using the total jump in magnetic and kinetic energies. Modifying the artificial viscosity term in this manner results in the addition of an explicit shear viscosity component. It is therefore somewhat undesirable to do so since this can result in excess spurious angular momentum transport elsewhere. A better approach would be to use divergence cleaning to prevent these errors from occuring. However, the hyperbolic cleaning was not found to be particularly effective for this problem because of the restriction to the fastest wave speed and implementation of the projection method is complicated by the periodic boundary conditions. These difficulties are not, however, insurmountable. The single biggest factor in determining the magnitude of the divergence errors in the shock tube tests was found to be the size of the smoothing region (ie. the number of contributing neighbours). It therefore seems advantageous to use a slightly larger number of neighbours for MHD problems (typically $h \gtrsim 1.5(m/\rho)^{1/\nu}$ where ν is the number of spatial dimensions) than might otherwise be used for hydrodynamics.

An MHD rotor problem was examined in §7.6, with results comparable to those shown in Tóth (2000). Finally the algorithm was tested on the Orszag-Tang vortex problem (§7.7) which has been widely used as a benchmark for MHD codes. The SPMHD results were in good agreement with those presented elsewhere. This test again highlighted the need for a slightly larger number of neighbours, in this case to remove spurious effects related to the initial lattice arrangement and to reduce the magnitude of the divergence errors. The hyperbolic/parabolic divergence cleaning was found to produce only a small reduction in the divergence errors, again highlighting the need for some form of sub-timestep cleaning (for example using the projection method).

An issue which has not been discussed in this paper, but which needs to be addressed elsewhere, is the tendency of SPH particles merge together at short separations due to the fact that the force tends to zero near the origin of the cubic spline kernel. In particular this problem can become more acute as the number of neighbours is increased (as is required in order to maintain the divergence constraint in MHD). This instability is well known but is not necessarily noticeable in SPH simulations, particularly in 3 dimensions, as it simply leads to a lower effective resolution. Whilst Thomas & Couchman (1992) propose a simple solution whereby the kernel gradient in the cubic spline is modified slightly whilst retaining the usual kernel for the density evaluation, it is not clear what effect this has on the evolution, particularly when using the variable smoothing length formalism which we have described here and in paper II. We therefore feel that this problem in particular warrants further attention.

Finally it is worth commenting on the ability of the algorithm as it stands to treat 'real' astrophysical MHD problems. The crucial issue here is the degree to which the divergence constraint can be maintained. Of the methods examined in this paper the most promising is the projection method using the Biot-Savart law since it is the only method which guarantees a zero divergence. Efficient implementation of this method in three dimensions requires use of a tree code (or similar) to solve the resulting Poisson-type equation similar to that used to compute the gravitational force. Note that the treecode implementation differs slightly from the usual gravity tree since the source term of the Poisson equation in this case is a vector quantity. Periodic boundary conditions add a further complication although again methods used for gravity can be easily adapted. Secondly the issue regarding particle merging discussed above needs to be addressed to be able to usefully increase the neighbour number. Thus, whilst many improvements could still be made to the algorithm, the results presented in this paper suggest that the method is ripe for application to problems of current theoretical interest, such as that of star formation.

ACKNOWLEDGEMENTS

DJP would like to especially thank Prof J.E. Pringle and Dr. M.R. Bate for numerous useful discussions. This work has been supported by PPARC, the Commonwealth Scholarship Commission and the Cambridge Commonwealth Trust.

REFERENCES

Balsara D. S., 1998, ApJS, 116, 133
Bekenstein J. D., Oron A., 2000, Phys. Rev. E, 62, 5594
Benz W., 1984, A&A, 139, 378
Benz W., Cameron A. G. W., Press W. H., Bowers R. L., 1990, ApJ, 348, 647
Brackbill J. U., Barnes D. C., 1980, J. Comp. Phys., 35, 426
Brookshaw L., 1985, Proceedings of the Astronomical Society of Australia, 6, 207
Byleveld S. E., Pongracic H., 1996, Publications of the Astronomical Society of Australia, 13, 71
Cerqueira A. H., de Gouveia Dal Pino E. M., 2001, ApJ, 560, 779
Cleary P. W., Monaghan J. J., 1999, J. Comp. Phys., 148, 227
Cummins S. J., Rudman M., 1999, J. Comp. Phys., 152, 584
Dahlburg R. B., Picone J. M., 1989, Physics of Fluids B, 1, 2153
Dai W., Woodward P. R., 1994, J. Comp. Phys., 115, 485
Dai W., Woodward P. R., 1998, ApJ, 494, 317
Dedner A., Kemm F., Kröner D., Munz C.-D., Schnitzer T., Wesenberg M., 2002, J. Comp. Phys., 175, 645
Dellar P. J., 2001, J. Comp. Phys., 172, 392
Evans C. R., Hawley J. F., 1988, ApJ, 332, 659

Gingold R. A., Monaghan J. J., 1977, MNRAS, 181, 375
Gray J., Monaghan J. J., Swift R. P., 2001, Computer methods in applied mechanics and engineering, 190, 6641
Hernquist L., Katz N., 1989, ApJS, 70, 419
Hosking J. G., 2002, PhD thesis, Cardiff University, UK
Janhunen P., 2000, J. Comp. Phys., 160, 649
Kuznetsov E. A., Ruban V. P., 2000, Phys. Rev. E, 61, 831
Londrillo P., Del Zanna L., 2000, ApJ, 530, 508
Meglicki Z., Wickramasinghe D., Dewar R. L., 1995, MNRAS, 272, 717
Monaghan J. J., 1992, Ann. Rev. Astron. Astrophys., 30, 543
Monaghan J. J., 1997, J. Comp. Phys., 136, 298
Monaghan J. J., Price D. J., 2001, MNRAS, 328, 381
Monaghan J. J., Price D. J., 2004, MNRAS, 350, 1449
Morris J. P., 1996, PhD thesis, Monash University, Melbourne, Australia
Morris J. P., Monaghan J. J., 1997, J. Comp. Phys., 136, 41
Morrison P. J., Hazeltine R. D., 1984, Physics of Fluids, 27, 886
Munz C.-D., Omnes P., Schneider R., Sonnendrücker E., Voß U., 2000, J. Comp. Phys., 161, 484
Orszag S. A., Tang C.-M., 1979, J. Fluid Mech., 90, 129
Phillips G. J., Monaghan J. J., 1985, MNRAS, 216, 883
Picone J. M., Dahlburg R. B., 1991, Physics of Fluids B, 3, 29
Powell K. G., 1994, Technical Report ICASE 94-24, An approximate Riemann solver for magnetohydrodynamics (that works in more than one dimension). NASA Langley Research center (available from http://techreports.larc.nasa.gov/ltrs/dublincore/1994/icase-1994-24.html)
Powell K. G., Roe P. L., Linde T. J., Gombosi T. I., de Zeeuw D. L., 1999, J. Comp. Phys., 154, 284
Price D. J., Monaghan J. J., 2004a, MNRAS, 348, 123
Price D. J., Monaghan J. J., 2004b, MNRAS, 348, 139
Price D. J., 2004, PhD thesis, University of Cambridge, Cambridge, UK (available from the author's website, currently at http://www.astro.ex.ac.uk/people/dprice)
Rosswog S., Davies M. B., Thielemann F.-K., Piran T., 2000, A&A, 360, 171
Ryu D., Jones T. W., 1995, ApJ, 442, 228
Ryu D., Jones T. W., Frank A., 1995, ApJ, 452, 785
Tóth G., 2000, J. Comp. Phys., 161, 605
Thomas P. A., Couchman H. M. P., 1992, MNRAS, 257, 11